Sedimentary cycling of zinc and nickel and their isotopes on an upwelling margin: Implications for oceanic budgets and paleoenvironment proxies

Journal Article

Author(s):
He, Zhiwei; Archer, Corey; Yang, Shouye; Vance, Derek

Publication date:
2023-02-15

Permanent link:
https://doi.org/10.3929/ethz-b-000592367

Originally published in:
Geochimica et Cosmochimica Acta 343, https://doi.org/10.1016/j.gca.2022.12.026

Funding acknowledgement:
165904 - Metal isotope constraints on biosphere-environment interactions in Earth history (SNF)
184873 - Using trace metal isotopes to understand ocean biogeochemistry: ancient and modern (SNF)

Geochimica et Cosmochimica Acta 343 (2023) 84–97

Contents lists available at ScienceDirect

Geochimica et Cosmochimica Acta

journal homepage: www.elsevier.com/locate/gca

Sedimentary cycling of zinc and nickel and their isotopes on an upwelling margin: Implications for oceanic budgets and paleoenvironment proxies

Zhiwei He [a,b,*], Corey Archer [a], Shouye Yang [b], Derek Vance [a]

[a] Institute of Geochemistry and Petrology, Department of Earth Sciences, ETH Zürich, Clausiusstrasse 25, Zürich 8092, Switzerland
[b] State Key Laboratory of Marine Geology, Tongji University, Shanghai 200092, China

ARTICLE INFO

Article history:
Received 20 April 2022
Accepted 24 December 2022
Available online 28 December 2022
Associate editor: Claudine Stirling

Keywords:
Zn isotopes
Ni isotopes
Porewater
Continental margin sediments
OMZ

ABSTRACT

Zinc and Ni are essential micronutrients whose stable isotope systematics in marine sediments represent promising, but still developing, tracers of past ocean chemistry and biology. Sediments from upwelling continental margins have been identified as important sinks for Zn and Ni, driven by high productivity, incorporation of the metals into cells and organic carbon burial. At present, however, our understanding of how Zn and Ni isotope composition of upwelling sediments reflects specific processes in the water column is incomplete. Here, we present coupled Zn and Ni abundance and isotope data for both solid phase and porewater in a series of sediment cores collected on a shelf-to-slope transect across an oxygen minimum zone (OMZ) from the southwest African margin off Namibia.

Zinc/Al and Ni/Al ratios in Namibian margin sediments are elevated relative to the lithogenic background, by factors of 1.4–2.4 and 1.7–5.7, respectively. Systematic relationships between solid phase Zn and Ni concentrations and organic carbon accumulation corroborate the view that authigenic Zn and Ni are mainly delivered to these sediments via export production from the photic zone. Corrections for detrital Ni are sometimes substantial, but authigenic δ^{60}Ni values are within uncertainty of the modern deep ocean, at 1.38 ± 0.18 ‰ (mean and 1SD, n = 42). Authigenic δ^{66}Zn is more variable, at −0.09 to 0.50 ‰, at or below the value for the deep ocean average. This latter observation can be attributed to Zn isotope fractionation during sequestration into authigenic ZnS phases in the sediments, either quantitatively, or partially.

Porewater systematics are more complex and the profiles do not necessarily reflect the redox state of the sediment-porewater system at the time of sampling, but rather characteristics inherited from more reducing conditions in a temporally heterogeneous system. Porewater zinc concentrations (30–369 nM) are much higher than the deep ocean and increase with depth beneath the sediment–water interface. Despite this prominent increase in Zn concentrations, δ^{66}Zn is rather constant and lighter than the deep ocean average, at 0.18 ± 0.06 ‰ (mean and 1SD, n = 33). These observations are most consistent with the buffering of the small porewater pool by the dissolution of a previously formed sulfide phase. Porewater Ni concentrations are closer to the deep ocean, mostly at 5–15 nM. The lightest porewater isotope compositions (δ^{60}Ni as low as 0.15 ‰) are consistent with a Mn-oxide source of Ni, whereas the heaviest isotope compositions (up to 1.76 ‰) clearly reflect uptake of light Ni into sulfide at depth within the sediment.

Our data, for the largest upwelling site in the modern ocean, add to sparse data from the eastern Pacific, and confirm that upwelling margin sediments bury Ni that is close to the deep ocean in isotope composition, but Zn that is generally lighter. The data thus confirm the importance of such margins in setting the heavy isotope composition of oceanic Zn. Sediments from this kind of setting hold significant potential for the construction of records of past oceanic Ni isotopes.

* Corresponding author at: Institute of Geochemistry and Petrology, Department of Earth Sciences, ETH Zürich, Clausiusstrasse 25, Zürich 8092, Switzerland.
E-mail address: hezw@tongji.edu.cn (Z. He).

https://doi.org/10.1016/j.gca.2022.12.026
0016-7037/

1. Introduction

The past couple of decades has seen increasing interest in the use of transition metals and their isotopes for investigating biogeochemical processes in the modern and ancient oceans. Zinc (Zn) and nickel (Ni), like other transition metals, are bioactive trace elements, both involved in a number of important enzymes required for marine phytoplankton (Morel and Price, 2003; Konhauser et al., 2009; Ragsdale, 2009; Twining and Baines, 2013; Morel et al., 2014). Consistent with their biological roles, Zn and Ni both show nutrient-type depth profiles in the ocean, closely correlating with those of macronutrients like phosphate and silica (Bruland, 1980). On the other hand, the behavior of both elements is sensitive to redox because their output fluxes are influenced by sorption to Fe–Mn oxides or removal as particulate sulfides (e.g., Tribovillard et al., 2006; Little et al., 2015). As a result, the biogeochemistry of Zn and Ni has motivated a new generation of studies on their isotope systems to provide constraints on the evolution of biological productivity and the redox history of the oceans (e.g., Kunzmann et al., 2013; Isson et al., 2018; Sweere et al., 2018, 2020; S.-J. Wang et al., 2019). These studies of Earth history must be underpinned by a thorough understanding of modern oceanic budgets, which still limits the reliable applications of such novel isotope systems to Earth history.

At a global scale, Zn and Ni isotope composition of seawater is determined by the amount and isotopic composition of different input and output fluxes (e.g., Cameron and Vance, 2014; Little et al., 2014). For Zn, at least remote from local sources such as hydrothermal systems (Conway and John, 2014; Lemaitre et al., 2020), the global deep ocean is isotopically homogeneous, at a δ^{66}Zn of 0.45–0.50 ‰. In contrast, the upper ocean, with extremely low Zn concentrations, is strongly skewed towards light Zn isotope values, either due to scavenging removal of heavy Zn or to inputs from external (anthropogenic) Zn sources (e.g., Bermin et al., 2006; Conway and John, 2014, 2015; Zhao et al., 2014; Samanta et al., 2017; John et al., 2018; Vance et al., 2019; R.-M. Wang et al., 2019; Lemaitre et al., 2020; Liao et al., 2020; Sieber et al., 2020). Previous work has highlighted the isotopically heavy deep ocean pool relative to the main inputs, which have a δ^{66}Zn of ~0.33 ‰, within the uncertainties of estimates for aeolian input and the upper continental crust (UCC; Little et al., 2014; Moynier et al., 2017). Dissolved Ni in the deep ocean is also isotopically uniform and heavier (at ~1.33 ‰ in δ^{60}Ni; Cameron and Vance, 2014; Takano et al., 2017; R.-M. Wang et al., 2019; Archer et al., 2020; Yang et al., 2020, 2021; Lemaitre et al., 2022) than the inputs (~0.7–0.8 ‰; Cameron and Vance, 2014; Revels et al., 2021). In common with other metal isotope systems, these budgets require an isotopically light output, or an unidentified heavy input, that drives the oceanic dissolved pool towards heavier values and maintains mass balance at steady state.

A number of studies have thus focused on the output fluxes, in order to quantify and understand the mass balance. The main outputs of both Zn and Ni (e.g., Maréchal et al., 2000; Gall et al., 2013; Little et al., 2014, 2016, 2020; Cameron and Vance, 2014; Vance et al., 2016; Ciscato et al., 2018; Gueguen et al., 2016, 2018, 2021; Gueguen and Rouxel, 2021) are via uptake into phytoplankton cells and burial of organic matter, particularly at upwelling margins, sorption to Mn oxides in the open ocean, and through sulfidation in euxinic setting such as the modern Black Sea. Our focus here is the first of these sinks, productive open-ocean upwelling margins. Organic-rich continental margin sediments are so far the only documented light removal sink for Zn from the open oceans (Little et al., 2016; Zhang et al., 2021). But this observation is based on only two studies and the mechanism controlling the sink is not clear. Some studies have emphasized the lack of Zn isotope fractionation during uptake into phytoplankton (e.g., Vance et al., 2016) and have suggested that low δ^{66}Zn values observed for these sediments may be the result of removal of Zn into sulfides. Others have suggested that there is potential for non-quantitative biological export of light organic Zn from the surface ocean (Isson et al., 2018; Weber et al., 2018). For Ni, only one study has sought to characterize the Ni output to organic-rich sediments at upwelling margins, demonstrating that organic-rich sediments at the Peru margin have δ^{60}Ni similar to modern seawater (Ciscato et al., 2018). As yet, the controls that determine the extent to which this output is driven by the two potential burial pathways – uptake in the photic zone during photosynthesis versus fixation in sulfide within the sediment – have not been evaluated in detail.

Here we present the first Zn and Ni isotope investigation of the sediment-porewater system for the upwelling margin off Namibia. The Namibian margin features one of the world's most intense upwelling regions, where Oxygen Minimum Zones (OMZs) develop with high rates of organic-carbon burial in response to enhanced primary productivity (Nelson and Hutchings, 1983; Shannon and Nelson, 1996). It also features a range of different redox conditions in sediment, which have been used to investigate redox-dependent variations of trace elements (Borchers et al., 2005; Abshire et al., 2020a) as well as several isotope systems (e.g., Fe, Mo, and U; Abshire et al., 2020b; Böning et al., 2020; He et al., 2021). In this study, the investigate stations on the Namibian margin represent shelf-to-slope settings across the OMZ, where the sediments are governed by a spectrum in environmental conditions, including redox. Our new dataset thus allows us to investigate the pathways of metal accumulation, retention and remobilization during early diagenesis under different boundary conditions, and their effect on sediment-porewater Zn and Ni isotope systematics.

2. Setting and samples

The Namibian margin, influenced by the Benguela Upwelling System (BUS), is one of the world's most productive coastal upwelling regions (Shannon and Nelson, 1996). The oceanography of BUS as part of the eastern boundary current system of the south Atlantic has been reviewed in a number of studies (e.g., Brüchert et al., 2006; Böning et al., 2020). Briefly, the Benguela current system consists mainly of a poleward Benguela undercurrent (BUC) and a broad equatorward flowing surface current with an oceanic (Benguela Oceanic Current, BOC) and a coastal (Benguela Coastal Current, BCC) branch descried in detail previously (Fig. 1; Nelson and Hutchings, 1983). The primary productivity of the BUS is sustained by the wind-driven upwelling of oxygen-depleted, nutrient-rich sub-surface South Atlantic central waters (SACW), which are transported southward by the undercurrent from the area of the subtropical Angola gyre (Mohrholz et al., 2008). Upwelling takes place along the entire coast of the Benguela area between 16°S and 34°S, but is most prominent in several upwelling cells. The Lüderitz cell (~26.5°S), just south of the study area, marks the strongest - and perennial - upwelling cell of the Benguela system.

Increased inflow of low-oxygen SACW into the BUS and respiration of organic matter strongly reduces the oxygen level of the waters, causing anoxic water-column conditions and thereby, resulting in the formation of an OMZ at around 150–450 m water depth over the Namibian shelf and upper slope (Monteiro et al., 2006; Mohrholz et al., 2008). The Namibian OMZ is generally considered to be highly dynamic, with its boundaries fluctuating temporally as a response to seasonal-interannual changes in upwelling intensities and productivity (Nagel et al., 2013). This creates conditions leading to seasonal oxygenation on the shelf during austral winter/spring. Under extreme oxygen deficient conditions during the highly productive austral summer, the shelf environment can

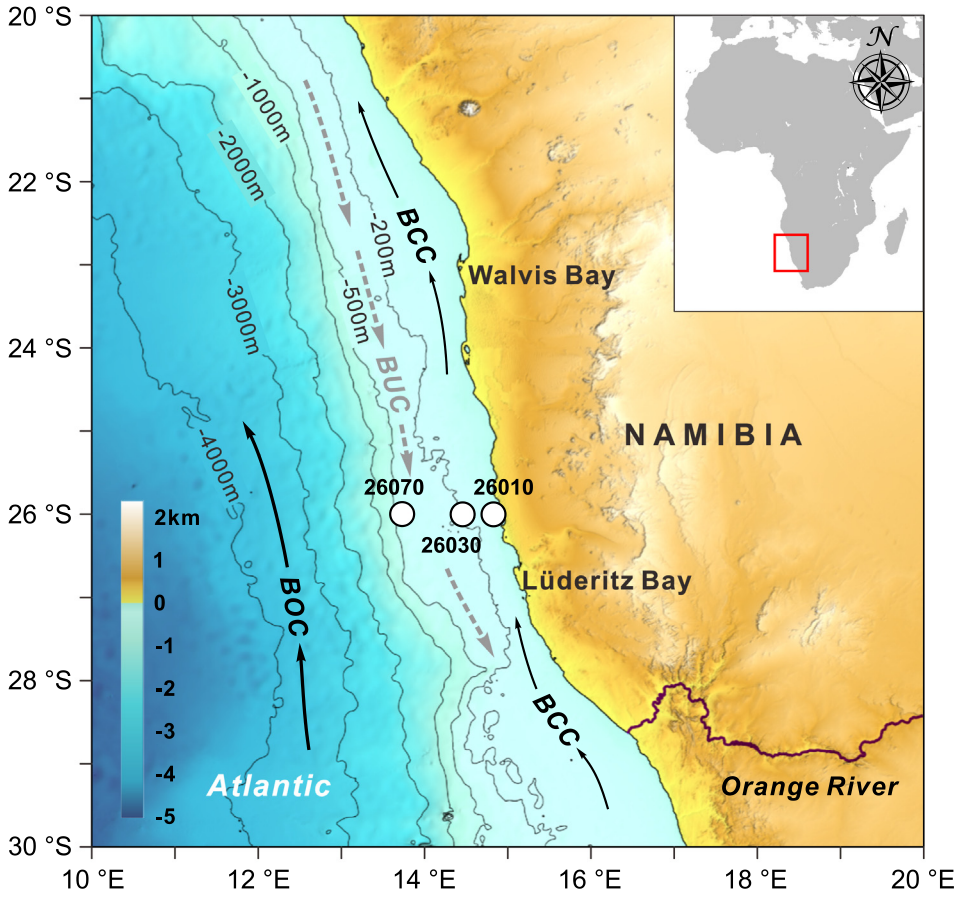

Fig. 1. Bathymetric map of the study area off Namibia, showing station locations on the 26°S transect. Schematic currents are modified from Inthorn et al. (2006a). The black arrows mark the main surface branches of the Benguela current system, including the Benguela Oceanic Current (BOC) and Benguela Coastal Current (BCC). The poleward Benguela Under-Current (BUC) over the outer shelf is marked by dashed grey arrows.

become reducing enough to allow for significant sulfide build-up in the sediment and, in some cases, even result in eruptions of H_2S gas to the water column (Weeks et al., 2004; Brüchert et al., 2006). Investigations have shown that episodical H_2S eruptions have immediate impacts on the biogeochemical cycles in the Benguela marine ecosystem, with direct precipitation of several metals in bottom water by reactions with sulfide (Borchers et al., 2005).

Sediments on the Namibian margin are subject to different depositional environments, varying from near-shore mud, through sandy shelf sediments, to fine-grained sediments on the upper slope. On the shelf there is a mud belt of diatomaceous ooze with up to 15 wt% organic carbon, representing the shelf depocenter for productivity in the Benguela system (Mollenhauer et al., 2002). The modern sediment flux into the Namibian shelf upwelling area is rich in biogenic components, including diatoms, foraminifera, and dinoflagellates (Hansen et al., 2014), with low terrigenous input from perennial fluvial sources such as the Orange River (Fig. 1; Bremner and Willis, 1993). In particular, high bacterial sulphate reduction rates coupled with limited oxidative precipitation of H_2S due to low concentrations of reactive iron has led to high accumulation of H_2S in shelf sediments - primarily in regions north of Lüderitz - favoring trace metal enrichment (Brüchert et al., 2003; Borchers et al., 2005). Though the slope sediments are often poor in organic carbon, reworking and lateral transport of shelf sediments to the slope in nepheloid layers occurs between 24.5°S and 26°S, resulting in a prominent depocenter of organic carbon on the slope in water depths of 400–1500 m (Inthorn et al., 2006a, 2006b).

We investigate short sediment cores from three sites on a transect along 26°S (see Fig. 1; Table 1), which were retrieved during cruises on Namibia's R/V MIRABILIS in April 2017. Hydrographic and water-column oxygen concentration data for this cruise transect are available in He et al. (2021). Stations 26010, 26030, and 26070 lie at the upper edge, within and below an OMZ (O_2- < 20 µmol/L) with the cores coming roughly from 100 to 500 m water depth (Table 1). Sediments analyzed in this study were collected using a multi-corer equipped with pre-drilled core tubes. Upon recovery, porewaters were extracted *in-situ* using Rhizon samplers at cm resolution (see full details: He et al., 2021). The extracted porewaters were then transferred into pre-cleaned 30 mL LDPE bottles, and acidified to pH < 2 with concentrated trace metal grade nitric acid. Solid sediment samples were sub-sectioned from an adjacent core at 1–5 cm depth resolution, then dried and homogenized using an agate pestle and mortar prior to chemical analysis. Some of the data used in this paper were published in He et al., 2021, including selected element concentration, total organic carbon (TOC), and pyrite Fe (Fe_{py}) contents in the sediment, as well as the porewater Fe, Mn, and H_2S data. Of importance to this study is that the three cores targeted here cover a range of sedimentary redox conditions and organic matter contents, related to export production.

3. Methods

Sample preparation and analysis were conducted in the clean lab at ETH Zürich. The porewater samples were weighed and then transferred to pre-cleaned Teflon beakers. An aliquot of each porewater sample was diluted x100 using 0.3 N nitric acid for the

Table 1
Position, water depth, bottom water oxygen concentration, depositional location for stations 26010, 26030, and 26070.

Station #	Latitude	Longitude	Water depth (m)	Bottom water O_2 (μmol/L)[a]	Depositional location
26010	26°00.007′S	14°46.467′E	116	10.70 (109 m)	inner shelf
26030	26°00.05′S	14°24.44′E	198	2.34 (197 m)	middle shelf
26070	25°59.986′S	13°40.251′E	509	58.21 (476 m)	upper slope

[a] Bottom water oxygen concentrations were detected by CTD. The bracket numbers refer to the water depth for CTD measurements.

determination of elemental concentrations. For the sediments, approximately 50–100 mg of the powdered samples was weighed. The samples were digested on a hotplate with a 4:1 mixture of concentrated HF and HNO_3, dried down to remove HF, refluxed in 6 N HCl to remove fluorides, and then re-dissolved in concentrated nitric acid with 10 vol% concentrated H_2O_2 to oxidize organic matter. Finally, the samples were brought up in 0.3 N nitric acid for elemental analysis. Elemental concentrations were obtained using a Thermo-Fisher Element XR sector-field ICP-MS after the addition of indium internal standard. Accuracy and precision were assessed using two secondary multi-element standards: the National Research Council of Canada river standard SLRS5, and USGS shale standard SGR1. The concentrations obtained matched certified values to within 5–10 % for the elements reported here.

Following concentration analysis, sediment sample aliquots containing a total of ~100–300 ng Zn and ~100–200 ng Ni were taken for isotope analysis. The sediment samples were spiked with ^{64}Zn–^{67}Zn and ^{61}Ni–^{62}Ni double-spikes to achieve a sample-spike ratio of approximately 1. Porewater samples were also spiked with the Zn and Ni double-spikes. After spiking, the porewater samples were dried down and re-dissolved in 7 N HCl. During this step, a large NaCl precipitate formed in porewater samples due to their high Na content. The supernatant was transferred into another pre-cleaned Teflon beaker. Yields obtained through comparison of the signal size from the isotope analysis with the Zn and Ni abundances defined by isotope dilution at the time of spiking indicate that the salt contained insignificant Zn and Ni. All spiked samples were then dried down and re-dissolved in 1 mL 7 N HCl + H_2O_2 in preparation for column chromatography.

The column procedure and analytical protocols for Zn and Ni isotope analysis have been described previously (e.g., Little et al., 2014, 2020; Zhao et al., 2014; Vance et al., 2016; Ciscato et al., 2018; Archer et al., 2020), and only a brief summary is given here. To separate individual transition metals from each other and from the matrix, the sediment and porewater samples were first passed through an anion-exchange column (Bio-Rad AG MP-1 M resin). This produces a relatively pure Zn fraction and an impure Ni fraction. This Zn fraction was further purified by a second pass through this anion column. The impure Ni fraction was first passed through a Nobias resin column to remove any residual Na, Mg or Ca remaining from the initial anion column. This column is a miniaturized version of the Nobias pre-concentration column used previously to concentrate trace metals from seawater (Takano et al., 2013, 2017; R.-M. Wang et al., 2019; Archer et al., 2020). A second step uses the cation exchange resin AG 50W X8 (Bio-Rad) to remove residual Al. The third and final step uses Re resin, to isolate Ni from residual Ti. Full details of the above described procedures in this group were recently given by Sun et al. (2021).

Zn and Ni isotope measurements were performed at ETH Zürich, using a Thermo Scientific Neptune Plus MC-ICP-MS in low-resolution mode. Samples were introduced into the mass spectrometer in 0.3 N HNO_3 via a Savillex C-Flow PFA nebulizer (50 μL min^{-1}) attached to a Teledyne-Cetac Aridus II desolvator. All Zn and Ni isotope compositions are given in standard notation relative to the JMC Lyon Zn and NIST SRM 986 standards, respectively, as follows:

$$\delta^{66}Zn = 1000\left[\frac{(^{66}Zn/^{64}Zn)_{sample}}{(^{66}Zn/^{64}Zn)_{LyonJMC}} - 1\right] \quad (1)$$

$$\delta^{60}Ni = 1000\left[\frac{(^{60}Ni/^{58}Ni)_{sample}}{(^{60}Ni/^{58}Ni)_{NISTSRM986}} - 1\right] \quad (2)$$

Long-term reproducibility of isotope analysis on the instrument is monitored by repeat measurement of secondary standard IRMM-3702 for Zn, and a primary NIST standard as well as a secondary standard (USGS Fe–Mn nodule, Nod-A1, digested and passed through the Ni column chemistry) for Ni. These give $\delta^{66}Zn$ = 0.30 ± 0.06 ‰ (2SD, n = 472) for IRMM-3702 and $\delta^{60}Ni$ = 1.04 ± 0.07 ‰ (2SD, n = 175) for Nod-A1 over the course of this and parallel studies, in agreement with previously published results in other laboratories (Gueguen et al., 2013; Moynier et al., 2017). The uncertainties shown on all figures are the long-term reproducibility, unless the internal uncertainty is larger, in which case the latter is shown. The total procedural blank was < 1 ng for Zn, and <0.2 ng for Ni. These blank contributions were negligible and not corrected for.

4. Results

4.1. Zinc and nickel in the solid phase

The chemical and isotope compositions of sediment are summarized in Table S1 and illustrated in Fig. 2. To account for contributions from the lithogenic (terrigenous) component, we calculated enrichment factors (EF) of Zn and Ni relative to the lithogenic background (Rudnick and Gao, 2003; Böning et al., 2012) as $X_{EF} = (X/Al)_{sample}/(X/Al)_{lith}$, where X and Al represent the concentrations by weight of element X and Al, respectively. The EF values for selected elements are presented in Table S1. Both Zn and Ni abundances show moderate authigenic enrichments over the lithogenic background (Fig. 2). It is worth noting that the authigenic fraction of Zn and Ni in marine sediments includes that associated with both biogenic (e.g., cellular and/or skeletal) particles and chemical (e.g., sulfide and/or oxide) precipitates. In detail, the inner shelf core (station 26010) exhibits relatively low Zn/Al ratios of 11.6 to 15.0, while the cores on the middle shelf and upper slope (stations 26030 and 26070) generally exhibit higher Zn/Al ratios of 16.5–17.6 and 15.1–20.0, respectively. Therefore, we observe a spatial trend in Zn_{EF}, which increases from ~1.6 for the inner shelf core to values in the range ~1.8–2.4 for the middle shelf and upper slope cores. Values for Ni/Al (5.5–8.2) in the inner and middle shelf cores are similar to each other with Ni_{EF} between 1.7 and 2.5. Those for the core on the slope are notably higher (Ni/Al: 10.0–18.7; Ni_{EF}: 3.0–5.7).

Each core presents relatively homogeneous Zn and Ni isotope compositions, but with significant differences between sites. Thus, $\delta^{66}Zn_{bulk}$ ranges from 0.26–0.35 ‰ for station 26010, from 0.18–0.26 ‰ for station 26030, and from 0.10–0.21 ‰ for station 26070. The $\delta^{60}Ni_{bulk}$ ranges from 0.69–0.90 ‰ for station 26010, from 0.50–0.66 ‰ for station 26030, and from 1.07–1.27 ‰ for station 26070.

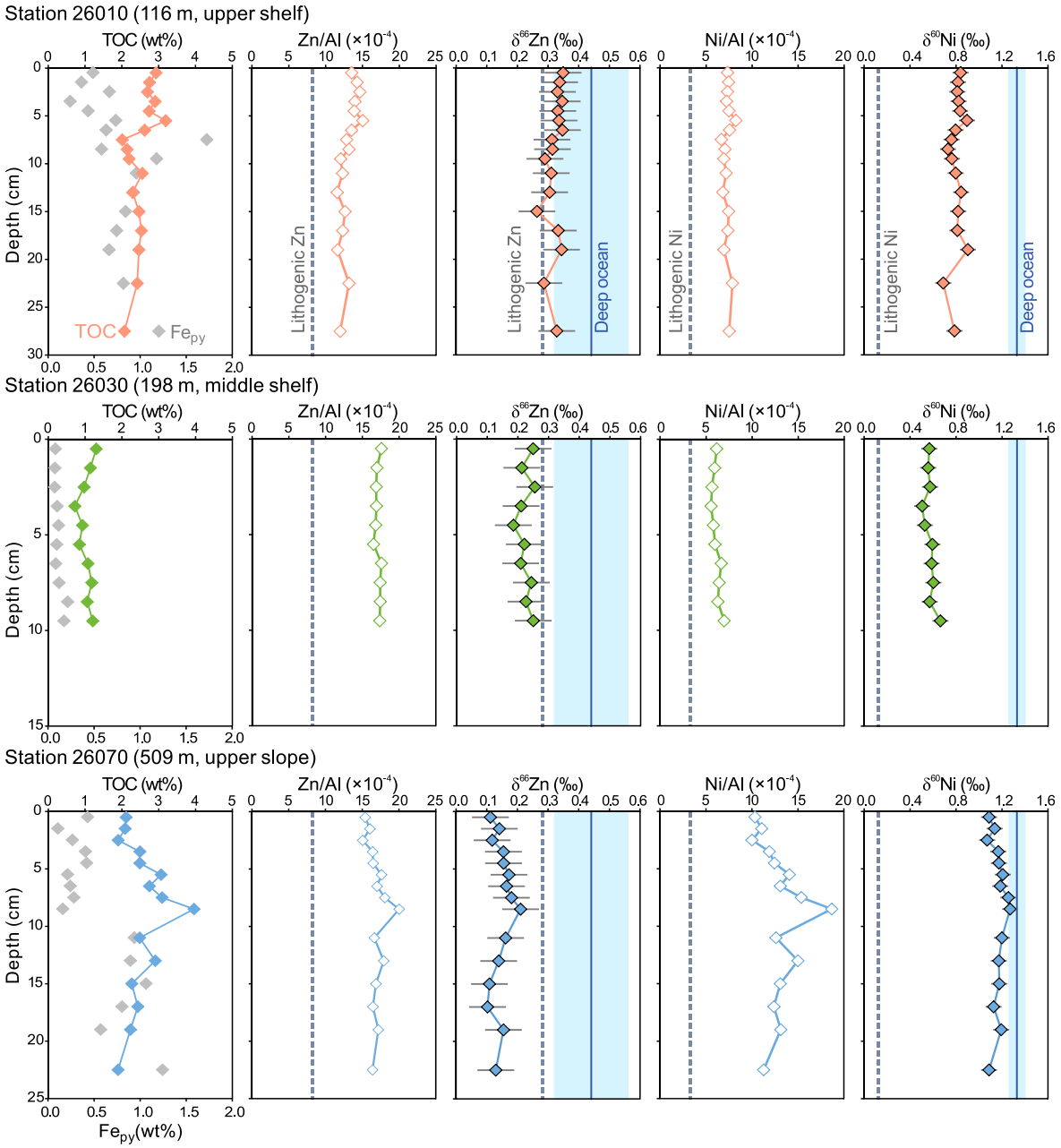

Fig. 2. Chemistry and isotope composition of the solid phase in Namibian margin sediments. The vertical dashed lines represent the average lithogenic Zn/Al (8.22×10^{-4}; Rudnick and Gao, 2003) or Ni/Al (3.3×10^{-4}; Böning et al., 2012) ratios, as well as the average lithogenic Zn (δ^{66}Zn = 0.28 ‰) or Ni (δ^{60}Ni = 0.12 ‰) isotope composition. The blue line and associated band on this and subsequent diagrams indicate the average and 1SD of the Zn (δ^{66}Zn = 0.44 ± 0.12 ‰) or Ni (δ^{60}Ni = 1.33 ± 0.07 ‰) isotope composition of the modern deep ocean (see the data compilations in Müsing et al., 2022; Lemaitre et al., 2022, respectively). All error bars on this and subsequent diagrams represent the 2SD reproducibility.

4.2. Zinc and nickel in porewaters

Zinc and Ni abundance and isotope compositions in porewaters, with dissolved Fe, Mn, and H_2S, are reported in Table S2 and shown in Fig. 3. At all stations, porewater Zn concentrations (30–369 nM) are elevated compared to typical seawater concentration (<10 nM) and generally increase with depth at all stations. The total range of dissolved δ^{66}Zn values spans from 0.05 to 0.29 ‰, with no systematic relationship to dissolved Zn concentrations. The Zn isotope compositions are slightly lighter in the inner shelf core 26010 (from 0.05 to 0.25 ‰) than in the other two cores (from 0.13 to 0.29 ‰). The dissolved Ni concentration and δ^{60}Ni in porewaters exhibit distinct down-core distribution patterns between stations. At station 26010, porewater Ni concentrations are low, at between 3.1 and 7.3 nM, within the range previously observed in seawater (~2–10 nM; Bruland, 1980; Cameron and Vance, 2014; Archer et al., 2020; Middag et al. 2020), while the dissolved δ^{60}Ni ranges between 0.15 and 0.76 ‰, decreasing downward coupled to an increase in H_2S and a slight increase in Ni concentration (Fig. 3). Porewaters from station 26030 display a narrow range in Ni concentration, between 5.4 and 13.4 nM, while δ^{60}Ni ranges from 0.25 to 1.32 ‰, generally increasing with depth. At station 26070, a decreasing trend in Ni concentrations with depth is interrupted by a very pronounced peak (up to 43.4 nM) centred on 8–

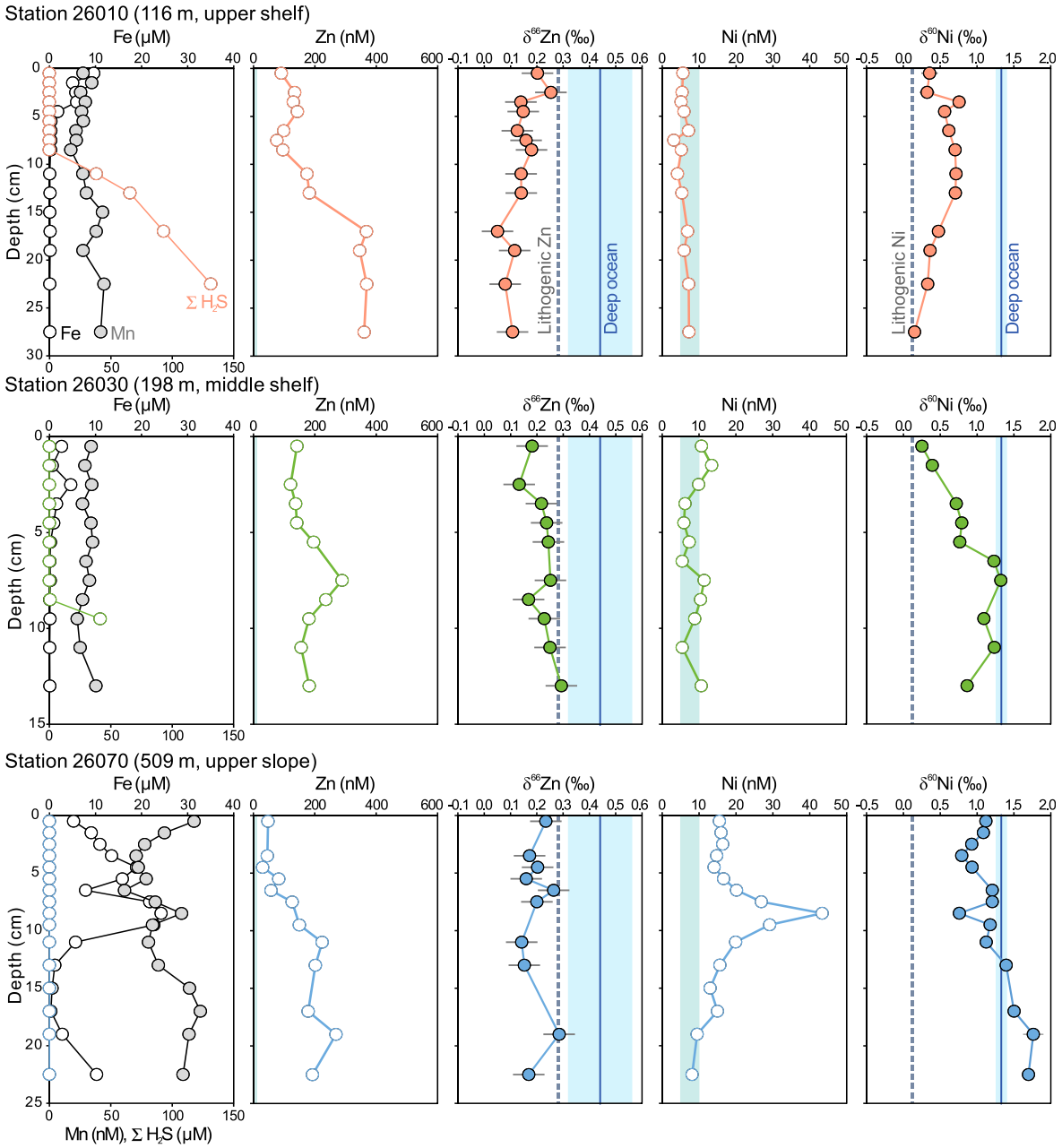

Fig. 3. Chemistry and isotope composition of porewaters in Namibian margin sediments. The vertical light green bands represent the typical range (5–10 nM) of dissolved Zn or Ni concentrations in seawater.

9 cm. Dissolved δ^{60}Ni values are relatively constant (0.79–1.21 ‰) for the near-surface (0–8 cm) porewaters, but then increase downward from 0.76 to 1.76 ‰.

5. Discussion

5.1. Detrital and authigenic Zn and Ni in Namibian margin sediments

In Fig. 4, bulk sediment δ^{66}Zn and δ^{60}Ni are plotted against Al/Zn and Al/Ni, respectively. There is no simple relationship between bulk δ^{66}Zn and Al/Zn in sediments, either for the data from our study sites or for literature data for the east Pacific upwelling margin and Long Island Sound in the North Atlantic (Fig. 4a; Little et al., 2016; Zhang et al., 2021). There is a suggestion in Fig. 4a that sediments deposited in less reducing environments (e.g., site 26030 and 26070; California and Mexican margin) exhibit lower δ^{66}Zn values than sediments from anoxic to mildly sulfidic settings such as our site 26010 and Peru margin. One plausible cause of this difference might be the degree to which the sequestration of isotopically light Zn to sedimentary sulfide is quantitative (Little et al., 2016). This would, in turn, suggest that the different depositional redox conditions, rather than detrital dilution, influence the Zn isotope fractionation during sequestration into the sediments. In contrast, the negative correlation for Ni can be explained, to first order, by two component mixing between a detrital pool and an authigenic Ni pool, the latter at Al/Ni close to 0 and with a δ^{60}Ni close to seawater, similar to the Peru margin (Fig. 4b; Ciscato et al., 2018).

The fractional contributions of Zn or Ni from authigenic sources to individual samples can be calculated as follows:

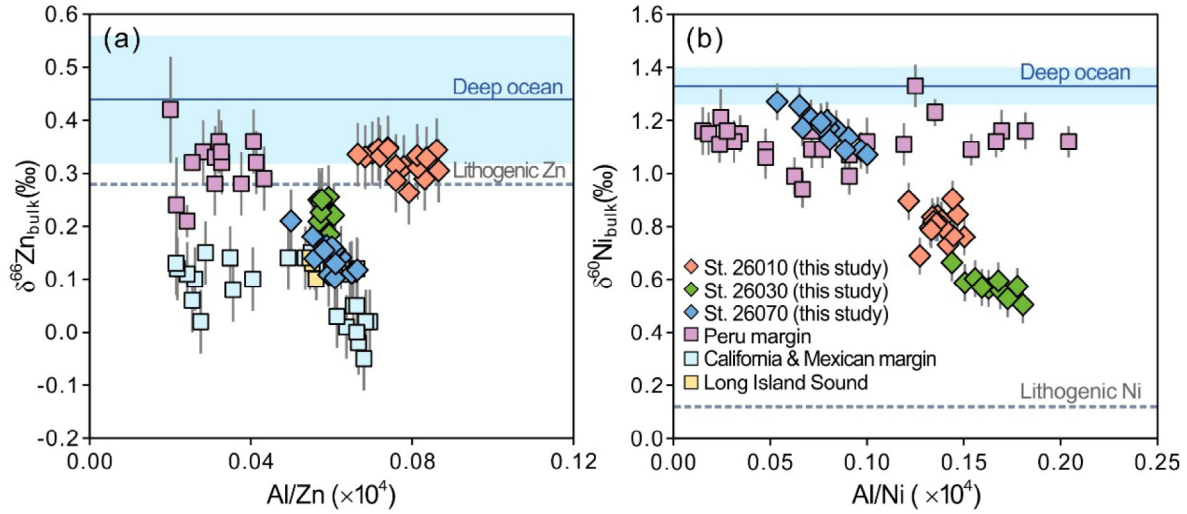

Fig. 4. Cross-plots of (a) δ^{66}Zn versus Al/Zn and (b) δ^{60}Ni versus Al/Ni for bulk sediments from the Namibian margin (diamonds) compared to data from other open-marine continental margins (squares). These latter are from the Peru, California and Mexican margins, and Long Island Sound (Little et al., 2016; Zhang et al., 2021) in panel (a), and from the Peru margin (Ciscato et al., 2018) in panel (b).

$$Zn_{auth}(\%) = (1 - [(Zn/Al_{det} \times Al_{bulk})/Zn_{bulk}]) \times 100 \quad (3)$$

$$Ni_{auth}(\%) = (1 - [(Ni/Al_{det} \times Al_{bulk})/Ni_{bulk}]) \times 100 \quad (4)$$

where Zn_{bulk}, Ni_{bulk}, and Al_{bulk} denote the bulk Zn, Ni, and Al concentrations of the sediment, Zn/Al_{det} and Ni/Al_{det} denote the ratios for detrital material. The accuracy of these authigenic Zn and Ni estimates depends on the choice of Zn/Al_{det} and Ni/Al_{det} ratios, which are known to vary regionally in the modern ocean (e.g., Böning et al., 2012; Little et al., 2015; Ciscato et al., 2018). In the absence of direct constraints on the detrital component of these sediments, we assume a Zn/Al_{det} of 8.22×10^{-4}, the ratio in the UCC (Rudnick and Gao, 2003; Little et al., 2016). However, as shown in Böning et al. (2012) and Ciscato et al. (2018), the UCC Ni/Al value does not represent that for Namibian and Peru margin sediments. Böning et al. (2012) use the intercept on a plot of Ni/Al ratio versus TOC to define the Ni/Al ratio of the detrital fraction. Here we assume Ni/Al_{det} of 3.3×10^{-4}, which represents an upper limit for upwelling regions (Böning et al., 2012; Ciscato et al., 2018). This estimate of the authigenic fraction (f_{auth}) of sedimentary Zn and Ni is then used to obtain the isotope composition of the authigenic sedimentary pool according to the following mass balance equations:

$$\delta^{66}Zn_{auth} = (\delta^{66}Zn_{bulk} - [(1 - f_{auth})\delta^{66}Zn_{det}])f_{auth}^{-1} \quad (5)$$

$$\delta^{60}Ni_{auth} = (\delta^{60}Ni_{bulk} - [(1 - f_{auth})\delta^{60}Ni_{det}])f_{auth}^{-1} \quad (6)$$

where $\delta^{66}Zn_{bulk}$ and $\delta^{60}Ni_{bulk}$ denote the bulk Zn and Ni isotope composition, $\delta^{66}Zn_{det}$ and $\delta^{60}Ni_{det}$ denote the isotope compositions of the detrital pools. A value for $\delta^{66}Zn_{det}$ and $\delta^{60}Ni_{det}$ is conventionally taken to be that of the global average isotope composition of detrital Zn (0.28 ± 0.07 ‰, 1 SD; Moynier et al., 2017) and Ni (0.12 ± 0.11 ‰, 1 SD; Cameron et al., 2009; Revels et al., 2021), respectively. We then use a Monte Carlo approach to evaluate the uncertainties on calculated $\delta^{66}Zn_{auth}$ and $\delta^{60}Ni_{auth}$ values (see details in Supplementary Material).

The estimated authigenic Zn fraction ranges from 29 to 59 %, with a $\delta^{66}Zn_{auth}$ of −0.09 to 0.50 ‰ (Fig. 5a-b). The inner shelf sediments at station 26010 have the lowest Zn_{auth} fraction of 29 to 45 % (Fig. 5a), so that the detrital correction is largest and values for $\delta^{66}Zn_{auth}$ are the least certain. Nevertheless, authigenic Zn isotope values (mean $\delta^{66}Zn_{auth}$ = 0.40 ± 0.07 ‰, 1SD, n = 17) are very close to global deep seawater (0.44 ± 0.12 ‰, data compiled in Müsing et al., 2022). In contrast, the upper slope sediments have much lower $\delta^{66}Zn_{auth}$, generally<0.1 ‰, while the middle shelf sediments have intermediate $\delta^{66}Zn_{auth}$ in the range of 0.08 to 0.24 ‰ (Fig. 5b). These $\delta^{66}Zn_{auth}$, extending from seawater to lighter values, are consistent with those from the east Pacific

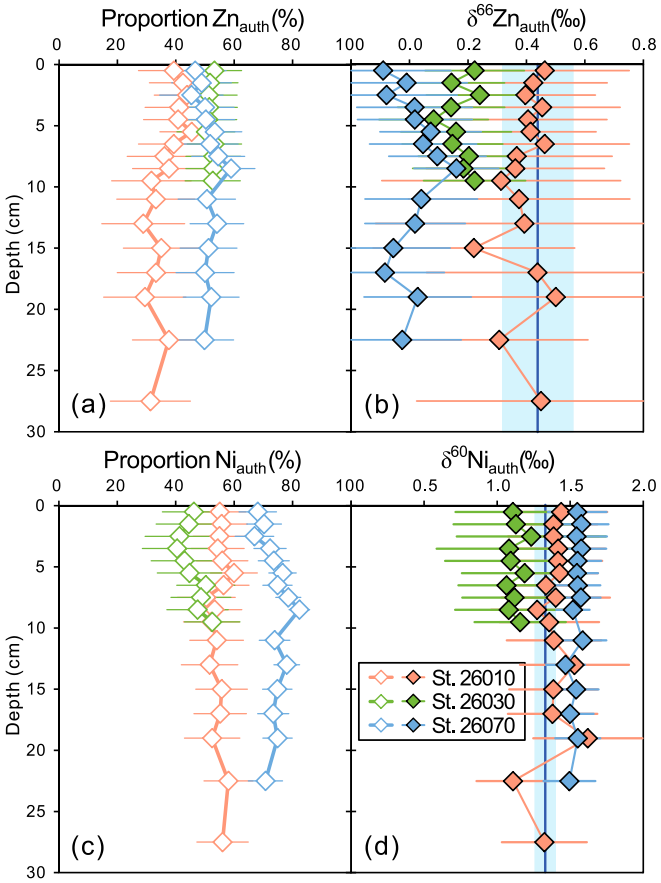

Fig. 5. Proportions of non-detrital Zn and Ni in sediments (left) and authigenic Zn and Ni isotope compositions (right).

margin (Little et al., 2016), and confirm the burial of light Zn in such upwelling settings. The same calculation demonstrates that 40–60 % the Ni accumulating in the sediments at stations 26010 and 26030, and up to 82 % at station 26070, is authigenic in origin (Fig. 5c), with Ni isotope values (1.38 ± 0.18 ‰, mean and 1SD, n = 42; Fig. 5d) that are within uncertainty of the deep open ocean (1.33 ± 0.07 ‰, data compiled in Lemaitre et al., 2022). These authigenic δ^{60}Ni are in good agreement with the inferred values through extrapolation to zero Al/Ni in Fig. 4b.

In summary, our study provides an important constraint on the distribution of authigenic Zn and Ni isotope compositions in different sediment localities beneath an OMZ on an upwelling margin. These observations raise key questions regarding the origin of authigenic Zn and Ni accumulation and associated isotope fractionation in open-ocean continental margin settings, discussed in detail below.

5.2. Mechanisms for authigenic Zn and Ni incorporation into Namibian margin sediments

In the most general terms, the two broad processes that could contribute to the authigenic pool identified in the previous section are: (1) transfer within the aqueous phase from the water column to porewater e.g., by diffusion, followed by sequestration from the porewater into an authigenic particulate phase and; (2) transfer via a particulate phase that sequesters Zn and Ni from the water column itself, and delivers it to the sediment-porewater system. A diffusive flux into the sediment-porewater system (e.g., Ciscato et al., 2018; Plass et al., 2021) appears to be ruled out in the case of these cores, at least for the conditions sampled here, given porewater Zn and Ni concentrations that are either much higher than seawater for Zn and close to seawater for Ni in two of the cores (Fig. 3). Of the particulate sources, it has been shown previously that Fe-Mn oxyhydroxides are very unlikely to deliver significant metals to the solid phase of Namibian sediments (He et al., 2021), given the lack of authigenic Mn enrichment as evidenced by the fact that Mn/Al ratios are uniformly below detrital value.

Zinc and other trace metals, such as Cu and Cd, are known to form solid sulfide precipitates in the ocean where sulfide is present (e.g., Morse and Luther, 1999; Janssen et al., 2014; Little et al., 2015). For example, the near quantitative removal of Zn in the deep sulfidic water column of the Black Sea has been attributed to the formation of particle-reactive $ZnS(HS)^-$ species, or association with a solid ZnS phase (Daskalakis and George, 1993; Vance et al., 2016). Though the removal of Ni into sulfides (Morse and Luther, 1999) is thought to be a significant sink for Ni in the deep Black Sea (Vance et al., 2016), it is much less important than for Zn, so that Ni is barely drawn down in the sulfidic water column of the deep Black Sea (Vance et al., 2016). Bottom water on the Namibian margin is not persistently sulfidic (Weeks et al., 2004; Brüchert et al., 2006), so that the potential delivery of Zn and Ni to Namibian sediment would require a more complex mechanism.

The significance of the sequestration of metals to sulfide formed in reducing particle-associated micro-environments within OMZ is debated (Janssen and Cullen, 2015; Vance et al., 2019; de Souza et al., 2022), and Yang et al. (2021) recently found little evidence of such a process for Ni. Though Namibian margin bottom waters are not persistently sulfidic, periodic H_2S eruptions are known to occur here (Weeks et al., 2004; Brüchert et al., 2006), in response to periods of strong upwelling and burial of organic matter. He et al. (2021) recently suggested that sequestration of Mo to sulfide during these events could play a role in the delivery of Mo to the Namibian sediment-porewater system. Fig. 6 compares Zn and Ni enrichment factors to those for Mo for the samples investigated here. Neither Zn nor Ni show any clear relationship with authigenic Mo enrichment, suggesting that sulfide precipitation in the water column is unlikely to be a significant mechanism for Zn or Ni accumulation in these sediments.

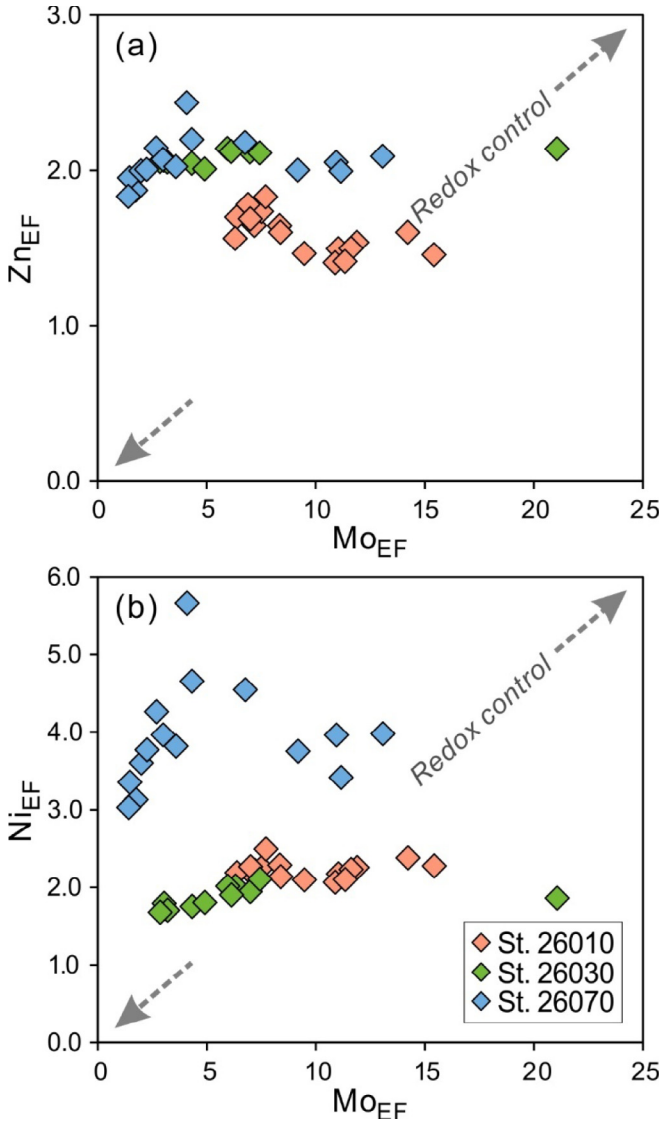

Fig. 6. Cross-plots of (a) Zn-Mo and (b) Ni-Mo enrichment factors (EF) for Namibian margin sediments. Mo EF is used as a proxy for local redox conditions. Data patterns imply that the mechanisms that have been suggested to enrich Mo in Namibian margin sediments (e.g., He et al., 2021) are not the dominant control on Zn and Ni authigenic enrichments.

Previous studies (e.g., Böning et al., 2012, 2015; Ciscato et al., 2018) have emphasized the role of Ni uptake into phytoplankton cells in the photic zone, and particulate organic matter as the key vector delivering Ni to upwelling margin sediments. This is supported by very strong relationships between Ni and TOC at both the Namibian and Peru margin, as well as a stoichiometric relationship between sedimentary Ni and total chlorins (the immediate degradation products of chlorophyll pigments; Böning et al., 2015). Similarly, Little et al. (2015) point to the correlation of sedimentary Zn with TOC as evidence that biological uptake and deposition of organic material is the main delivery pathway of Zn to sediments on the Peru margin.

This vector is investigated for the samples studied here in Fig. 7. Ratios of authigenic Zn to TOC (see the slope of arrays in Fig. 7a; Table S3) vary from core to core. Sediments from core 26010 and 26070 have a similar range of Zn/C with a mean of ~147 μmol/mol (Fig. 7a). A much higher Zn/C ratio (~385 μmol/mol) characterizes

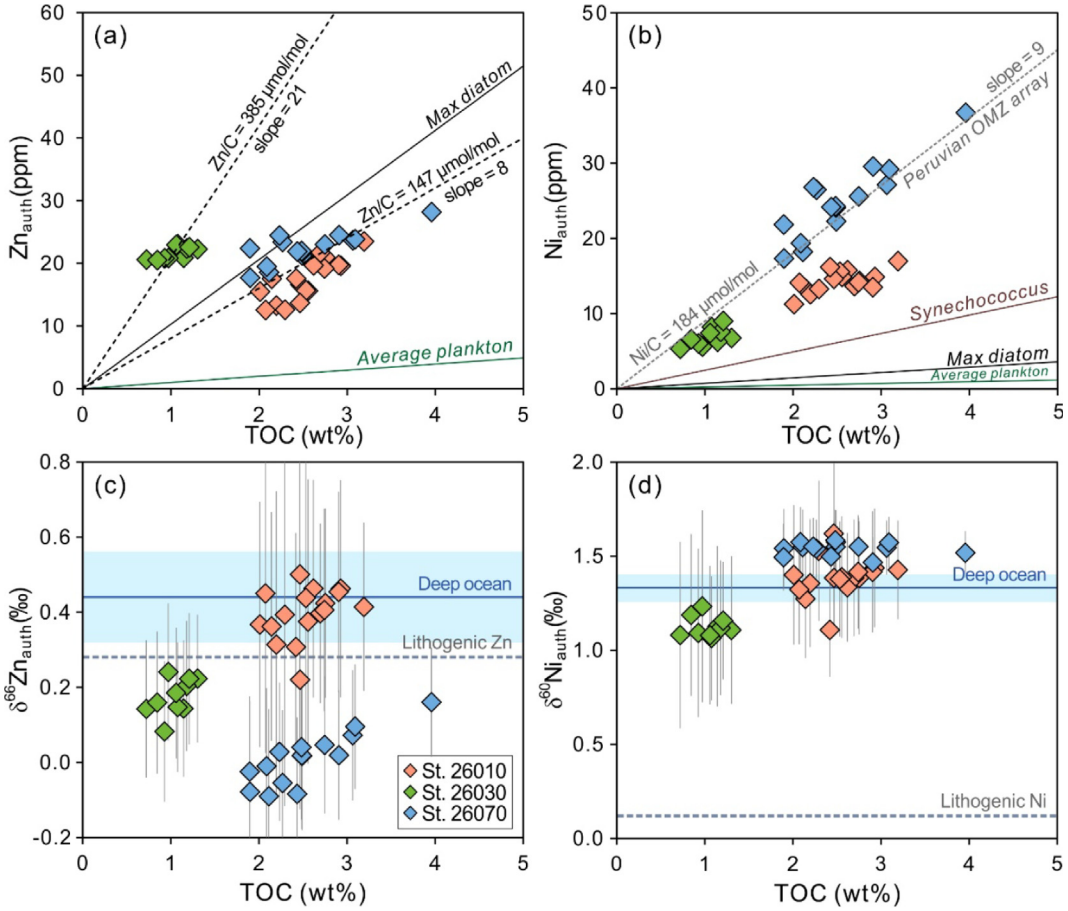

Fig. 7. Cross-plots of (a) Zn_{auth}, (b) Ni_{auth}, (c) $\delta^{66}Zn_{auth}$, and (d) $\delta^{60}Ni_{auth}$ versus TOC for Namibian margin sediments. In panel (a), the solid line represents the average Zn/C ratio (18 μmol/mol) in phytoplankton and the max Zn/C ratio (189 μmol/mol) in diatoms (Twining and Baines, 2013), respectively. The dashed lines with slopes of 8 and 21 denote the mean Zn/C ratio of sediments from core 26010 and 26070 and sediments from core 26030, respectively. In panel (b), the solid line represents the average Ni/C ratio (5 μmol/mol) in phytoplankton, the max Ni/C ratio (15 μmol/mol) in diatoms (Twining and Baines, 2013), and the Ni/C ratio (50 μmol/mol) in prokaryote *Synechococcus* (Twining et al., 2010), respectively. The dashed line represents the Ni-TOC array (with a slope of 9) defined by sediment data from the Peruvian OMZ (Böning et al., 2015; Ciscato et al., 2018). See text for discussion.

core 26030 (Fig. 7a). For comparison, scarce data for Zn/C ratios in phytoplankton range up to about 200 μmol/mol (Twining and Baines, 2013), with the highest values seen in diatoms, which dominate the Namibian margin. Correlations between Ni and TOC in upwelling margin sediments are strong (Böning et al., 2015; Ciscato et al., 2018), and the data presented here lie on an array with similar slope to that obtained previously, equivalent to a Ni/C ratio of 120–200 μmol/mol for most samples (Fig. 7b; Table S3). This range of Ni/C is much higher than that reported for diatom cells (up to ~15 μmol/mol; Twining and Baines, 2013). As noted by Ciscato et al. (2018), this large discrepancy cannot be solved by accounting for the Ni content of diatom opal (Twining et al., 2012), especially given recent data that suggest minimal incorporation of Ni into opal (John et al., 2022). Recently, it has been suggested that Ni uptake in the extra-polar photic zone is dominated by prokaryotic organisms (e.g., Archer et al., 2020; Yang et al.; 2020; Lemaitre et al., 2022). Again, data are scarce, but Ni/C ratios as high as 50 μmol/mol have been reported for *Synechococcus* (Twining et al., 2010).

In summary, the data presented here for the Namibian margin re-emphasize the previous finding (e.g., Böning et al., 2015; Little et al., 2015; Ciscato et al., 2018) that organic matter export from the photic zone is likely a key pathway for Zn and Ni supply to continental margin sediments. However, and as noted by Ciscato et al. (2018) for the Peru margin, metal/C ratios in sediment are definitely higher than, or at the high end of, ratios measured in phytoplankton cells collected from the upper water column. On the other hand, as also noted by Ciscato et al. (2018), sedimentary metal/C ratios are likely to be impacted by preferential remineralization of carbon relative to the metals. Differential remineralization of major components of cells – e.g. C, P – is well-established (e.g., Ingall and Jahnke, 1994; Paytan and McLaughlin, 2007).

5.3. Controls on authigenic $\delta^{66}Zn$ and $\delta^{60}Ni$ in Namibian margin sediments

5.3.1. Controls on $\delta^{66}Zn_{auth}$

Namibian margin sediments possess a range of authigenic $\delta^{66}Zn$ signatures, between −0.09 and 0.50 ‰, similar to or lighter than the deep ocean $\delta^{66}Zn$. Following Little et al. (2016), we consider two possible origins for the authigenic $\delta^{66}Zn$ signatures, and the variation away from water column signatures: (1) isotope fractionation associated with removal from the aqueous phase to particulates, during biological uptake or via scavenging; and (2) isotope fractionation within the sediment during early diagenesis of Zn.

Though the Zn isotope composition of the local water column is not available here, zinc upwelled into the photic zone from beneath the surface is expected to have the $\delta^{66}Zn$ of the deep ocean, at ~0.44 ‰. Particulate-associated scavenged Zn would be expected to be heavier than this deep ocean value (John and Conway, 2014), whereas authigenic Zn isotopes in Namibian margin sediments are either the same as the deep ocean or lighter

(Fig. 7c). It is well-established that diatoms dominate the phytoplankton ecology in the upwelling system off Namibia (Borchers et al., 2005), and Fig. 7a suggests that sedimentary Zn/C ratios are close to the highest values seen in diatoms. There is little evidence from the modern water column for the uptake of light Zn into phytoplankton cells (though see Samanta et al., 2017). In particular, Zn isotopes in residual surface seawater north of the diatom-dominated upwelling zone in the Southern Ocean barely change, despite the removal of about 99 % of the upwelled Zn pool into diatom cells (Zhao et al., 2014; R.-M. Wang et al., 2019; Sieber et al. 2020). For example, the extensive dataset in Sieber et al. (2020) suggests a maximum fractionation upon uptake of 0.06 ‰. Culturing studies of diatoms also suggest very small fractionations during uptake at the free Zn concentrations relevant to the oceans (John et al., 2007; Köbberich and Vance, 2017) and Köbberich and Vance (2019) suggest that even these small fractionations are artefacts of the complexation of Zn by very strong organic ligands in culture. It thus seems likely that biological particulates transport Zn to the sediment that is close to the isotope composition of the deep ocean.

The alternative explanation for light authigenic Zn in sediments (e.g., Little et al., 2016; Zhang et al., 2021) is that biological export from the photic zone delivers Zn to the sediment that is unfractionated from water column isotope compositions, and that it is diagenetic re-processing of this Zn that is the main control on isotope compositions. Specifically, Little et al. (2016) hypothesize release of Zn to porewaters via continued respiration of organic matter in the sediment, followed by preferential sequestration of light Zn into ZnS (e.g., Ducher et al., 2018) below the sulfate-reduction front, with diffusion of the heavier Zn isotopes back to seawater.

In principle, it is possible to interrogate this hypothesis through examination of porewater profiles and their relationship with the solid phase of the sediment. Zinc concentrations in porewaters are mostly much higher than seawater values at the sites studied here (Fig. 3), suggesting that release of Zn to porewaters is indeed occurring in these sediments. However, porewater Zn concentrations continue to increase downwards at depths where aqueous H_2S is detectable (e.g., site 26010, Fig. 3). This observation is consistent with recent data for porewater profiles in sediments within the OMZ off Peru (Plass et al., 2021) where, despite H_2S concentrations reaching up to 1000 μM, there does not appear to be visible Zn depletion with increasing core depth. Thus, in the scenario under consideration, uptake of Zn into new authigenic phases such as sulfide would need to be more than balanced by release of Zn from regenerated cellular material.

To the extent that it can be estimated precisely, given the uncertainties in the detrital correction, $\Delta^{66}Zn_{authigenic\text{-}porewater}$, shows systematic relationships between cores. For upper shelf site 26010, authigenic Zn is heavier, with $\Delta^{66}Zn_{authigenic\text{-}porewater}$ = 0.27 ± 0.08 ‰ (average and 1SD for all samples for which both solid phase and porewater data exist). At middle shelf site 26030 authigenic and porewater Zn have identical isotope compositions (with $\Delta^{66}Zn_{authigenic\text{-}porewater}$ = −0.03 ± 0.08 ‰. For upper slope site 26070 it is lighter, with $\Delta^{66}Zn_{authigenic\text{-}porewater}$ = −0.18 ± 0.08 ‰. These Δ values are almost completely controlled by differences in the authigenic component of the solid phase, given porewater values that vary little, despite a factor of > 6 variation in porewater Zn concentrations. The only explanation of this pattern that seems plausible is that the small porewater Zn reservoir is buffered by the dissolution of a single phase within the authigenic Zn pool. Given the conclusions of previous studies (Little et al., 2016; Zhang et al., 2021), it seems unlikely that this phase is organic.

A study of Mo and U in these same samples (He et al., 2021) uncovered complex porewater depth profiles that can only be explained by the temporally-variable sedimentary redox conditions that are characteristic of the Namibian upwelling system (e.g., Borchers et al., 2005; Böning et al., 2020), so that the sampled profiles represent a snapshot that does not conform to a steady-state scenario. Thus, pronounced peaks in porewater Mo and U concentrations at depth can only be explained by initial precipitation of a reduced solid phase under more reducing conditions prevailing prior to sampling, possibly associated with transiently high dissolved sulfide (Weeks et al., 2004; Brüchert et al., 2006) near the sediment–water interface, followed by dissolution of that phase under more oxidizing conditions before and at the time of sampling. It seems highly likely that these more complex scenarios affect the Zn data as well. For example, the porewater data at site 26010 is characterized by a kick at about 8 cm, beneath which Zn concentrations increase sharply, coincident with an increase in dissolved sulfide and a drop in $\delta^{66}Zn$. These data seem to be consistent only with a disequilibrium scenario, whereby previously-precipitated solid sulfide is now dissolving in response to oxidizing conditions at the top of the core, releasing light Zn and H_2S to porewaters.

In summary, the data presented here clearly confirm that authigenic Zn in productive upwelling margin sediments is isotopically light relative to the water column. We tentatively concur with previous studies (Little et al., 2016; Zhang et al., 2021), that this feature is unlikely to be due to the delivery of light Zn via uptake of Zn into cells and export to the sediment, and that it most likely results from diagenetic re-processing of cellular Zn taken up in the photic zone without isotope fractionation. However, the data we present do not clearly constrain the specific mechanism which leads to the retention of light Zn in the sediment. Such a constraint, given the multiplicity of possible diagenetic transformations that can occur, coupled to temporal heterogeneity in sedimentary redox state, will ultimately require more detailed observations and a diagenetic reactive transport model.

5.3.2. Controls on $\delta^{60}Ni_{auth}$

The Ni isotope data for the solid phase of these samples is much simpler than those for Zn. The bulk sediment data are readily explained by two-component mixing (Fig. 4b) between a detrital end-member with high Al/Ni and a low $\delta^{60}Ni$, and an authigenic end-member at low Al/Ni and a $\delta^{60}Ni$ close to the deep ocean (1.33 ‰). Though Fig. 5d and Fig. 7d suggest that the isotope composition of this authigenic end-member varies between 1.1 and 1.6 ‰, the uncertainties associated with the detrital correction are large for samples at the lower end of this range (site 26030) – at Ni/Al < 10×10^{-4} g/g. These findings are very similar to those of Ciscato et al. (2018) for the Peru margin, where sediments with Ni/Al > 10×10^{-4} g/g are clearly identical to the deep ocean in $\delta^{60}Ni$ whereas those with lower Ni/Al ratios yield larger uncertainties in $\delta^{60}Ni_{auth}$. Though all samples have $\delta^{60}Ni_{auth}$ that are within uncertainty of the modern deep ocean, it is possible that the values at the higher end of the range reflect the higher surface ocean $\delta^{60}Ni$ that is increasingly recognized as a feature of the low latitude oceans (Takano et al., 2017; Archer et al., 2020; Yang et al., 2020, 2021; Lemaitre et al., 2022).

Porewater Ni concentration and isotope data, as for Zn, Mo and U (this study, He et al., 2021), are more difficult to interpret in a straightforward manner. The upper slope site stands out as featuring higher Ni concentrations, with a pronounced peak at 8–9 cm and Ni isotope compositions that are both above and below the deep ocean value (Fig. 3). At this site, beneath the pronounced porewater peak at 8–9 cm, Ni concentration and isotope compositions change rapidly downwards (Fig. 3). This observation may be closest to a control by a single process: diffusion downwards to an authigenic sink with a preference for the light isotope at depth, perhaps beneath the sampled depth interval. This may reflect preferential removal of isotopically light Ni into a sulfide (Fig. 8), which

seems to match the isotope effect with a fractionation of approximately −0.66 ‰ from theoretical calculations (Fujii et al., 2011).

In contrast to the deeper portion of core 26070, δ^{60}Ni in the upper portion of this core, and at the shelf sites, is mostly distinctly lower than the deep ocean, extending down to about 0.1 ‰ (Fig. 3). A source that could produce the observed isotope shift from seawater, while barely affecting Ni concentrations (sites 26010, 26030; Fig. 3), would need to have an extremely light Ni isotope composition. Manganese oxides are expected to be isotopically light (Sorensen et al., 2020) and, in theory, represent one such source. Indeed, Vance et al. (2016) interpreted similarly extreme changes in δ^{60}Ni close to the Black Sea chemocline, also associated with much more subtle variation in Ni concentrations, in terms of Mn oxide cycling.

As noted previously, Namibian margin sediments have very low concentrations of Mn in both solid phase and porewater (Fig. 3; He et al., 2021). However, the important difference for Ni versus other metals such as Mo, U (He et al., 2021) and Zn (this study), is that Ni/Mn ratios in Mn oxides are very high, at 0.02 ± 0.01 mol/mol (Manheim and Lane-Bostwick, 1989). Porewater Mn concentrations in these cores of 50–100 nM (Fig. 3), presumably derived from reductive dissolution of Mn oxides within the sediment, could thus be associated with Ni addition of 1–2 nM if Ni release is quantitative, representing 7–64 % of porewater samples from sites 26010 and 26030. Natural and experimental data (Vance et al., 2016; Sorensen et al., 2020) suggest that Ni adsorbed to Mn-oxide can be 3–4 ‰ lighter than the aqueous phase they derive from. If this aqueous phase is the deep ocean, then Mn oxides could have δ^{60}Ni as low as −1.7 to −2.7 ‰. If such extreme Ni isotope compositions are relevant here, Mn-oxide associated Ni could shift porewater δ^{60}Ni downwards from seawater by 0.5–2.5 ‰, readily explaining the porewater data for the upper levels of core 26070 and the data for the other two sites.

There are other features of the porewater data that support the above inference, but also features that imply more complexity. For example, the Ni concentration peak at 8–9 cm in core 26070 is associated with a peak in porewater Fe and Mn. On the other hand, unlike for cores 26010 and 26030, this concentration peak is associated with only a minor shift in δ^{60}Ni (Fig. 3). But the impact of Mn-oxide associated Ni on porewater isotope compositions will be complicated by the degree to which Mn oxide dissolution is quantitative. For example, near quantitative dissolution of solid phase Mn oxide would release very light Ni to porewaters, whereas non-quantitative dissolution could, in principle, lead to retention of light Ni isotopes on residual Mn oxide solid such that the Ni released to porewater is heavier. This potentially explains the fact that porewater Ni is lightest at the more reducing sites studied here (Fig. 3; 26010 and 26030), sites that might be expected to see quantitative dissolution of Mn oxides, whereas the impact at the more oxidizing site (26070), where non-quantitative dissolution of Mn oxide is expected, is not as clear.

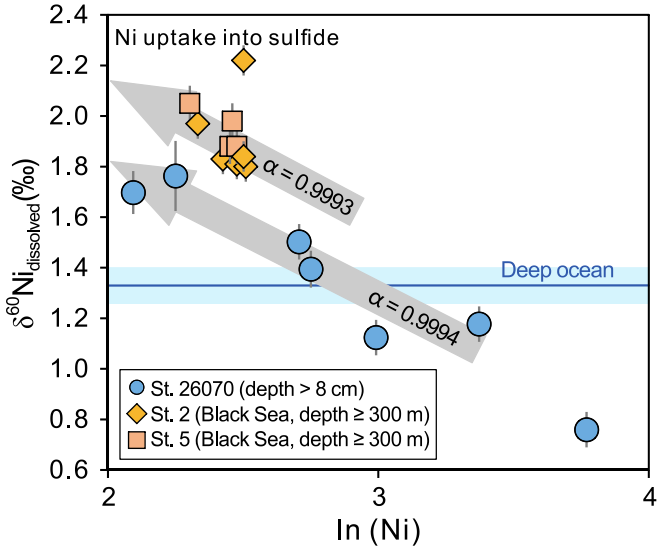

Fig. 8. Cross-plot of δ^{60}Ni versus ln (Ni) for porewaters below 8 cm from station 26070. The arrow indicates a Rayleigh fractionation trend towards lower [Ni] and higher δ^{60}Ni values, reflecting Ni uptake into a secondary authigenic sulfide phase at depth. Data documenting a similar process in the water column of the Black Sea (Vance et al., 2016) are shown for comparison.

5.4. Continental margins and the marine Zn-Ni isotope budgets, past and present

Ultimately and with further investigation, we suggest that porewater data will aid in gaining a better understanding of the specific mechanisms responsible for, e.g., the putative diagenetic reprocessing of Zn, which is thought to control the light isotope signature of authigenic Zn at continental margins. However, porewater data are complex for three main reasons. First, there is an array of potential diagenetic sources and sinks that control porewater metal abundances and isotope compositions. Second, the instantaneous profiles at the time of collection do not appear to be representative of the long-term situation, given the temporal variability in upwelling, primary productivity and organic carbon transfer to the sediment. Finally, the porewater metal reservoir is small relative to the much larger solid pool, making it very sensitive to multiple, temporally-variable, processes that are difficult to deconvolve. In this section, we focus mainly on the larger-scale implications of the solid phase data, for modern isotope budgets and for sedimentary records of Earth history.

The preceding results and discussion confirm conclusions made before for upwelling margins, though the addition of the Namibian margin data to previously sparse observations is important. Upwelling margin sediments clearly bury Zn that is isotopically lighter than the deep ocean dissolved pool (c.f., Little et al., 2016; Zhang et al., 2021) and Ni that is isotopically very close to the deep ocean (c.f., Ciscato et al., 2018). In agreement with previous studies (Böning et al., 2012, 2015; Little et al., 2016; Ciscato et al., 2018; Zhang et al., 2021) we suggest that organic matter export from the photic zone represents a major pathway of both Zn and Ni supply into the sediments, leading to strong Ni–TOC relationships (Fig. 7b), though Zn–TOC correlations are more complex (Fig. 7a). Authigenic δ^{60}Ni at upwelling margins shows a small range that is close to the modern deep ocean, consistent with previous finding for the biological Ni sink at the Peru margin (Ciscato et al., 2018). Authigenic δ^{66}Zn is more variable between the Namibian stations. In the end, however, the dataset presented here does not significantly change the conclusion in Little et al. (2016) concerning the burial of light Zn in such settings, and their importance for the global oceanic mass balance of Zn isotopes.

Recent studies (Little et al., 2020; Gueguen et al., 2021) have suggested that the heavy Ni isotope composition of seawater results from a heavy diagenetic source of Ni, related to the diagenetic transformation of Mn oxides in sediments of the oxic deep ocean. The porewater data for site 26070 raise the possibility of another mechanism for the supply of heavy Ni isotopes to the oceans through diagenesis: the uptake of light Ni isotopes into sulfide (Figs. 3 and 8). In the Black Sea, this process occurs in the water column (Vance et al., 2016), but is of minor importance for the global ocean mass balance given the very low rate at which seawater is processed through such settings. Though future work will need to confirm, two things make it likely that it is also of minor importance on upwelling margins. First, the areal extent of

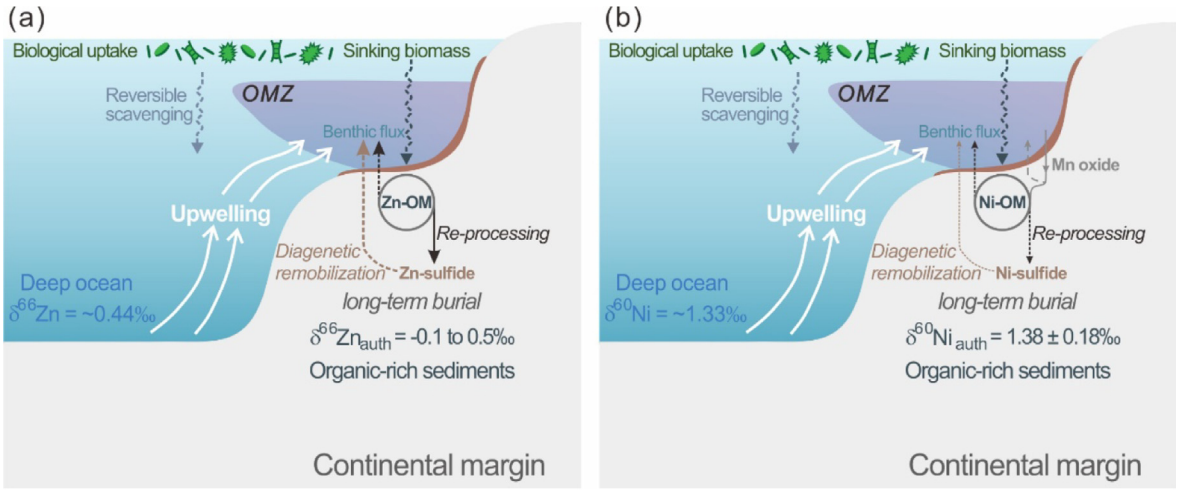

Fig. 9. Schematic illustrations of the mechanisms that control the burial and isotope compositions of (a) Zn and (b) Ni in continental margin sediments, as presented in this study. For both Zn and Ni, organic matter export from the photic zone represents a key delivery pathway to the sediments with little isotope fractionation. (a) Authigenic δ^{66}Zn results from diagenetic re-processing of cellular Zn and its sequestration into ZnS phases, associated with a corresponding heavy pool of dissolved Zn in porewaters. On the other hand, light dissolved δ^{66}Zn values and elevated Zn concentrations would be generated in porewaters via oxidative dissolution of sulfide under less reducing conditions. (b) Authigenic δ^{60}Ni, with values that are within uncertainty of the deep open ocean, suggests the re-processing of cellular Ni and its sequestration into sulfide phases and associated isotope fractionation is less important. Unlike Zn, Mn oxides have a fundamental role in the sedimentary cycling of Ni, contributing to light dissolved δ^{60}Ni in porewaters upon Mn oxide reduction.

these settings is small. Second, the degree to which it has an impact on the water column depends on the redox state at the seawater interface itself. At site 26070, for example, the depth interval where this process is important is overlain by an interval where any signal from it is mixed with a signal from different processes. However, in situations where porewater sulfide generation is close to the sediment–water interface, it may be more important.

As outlined in the introduction, sedimentary Zn and Ni isotope records may serve as tracers that enable reconstruction of past nutrient cycling and ocean chemistry (e.g., Liu et al., 2017; John et al., 2017; Sweere et al., 2018, 2020; S.-J. Wang et al., 2019; Yan et al., 2019; Chen et al., 2021; Li et al., 2021; Zhao et al., 2021). It is clear from this study, and that on the Peru margin of Ciscatio et al. (2018), that records of authigenic Ni isotopes at upwelling margins have great potential for recording the δ^{60}Ni of contemporary seawater. On the other hand, our results highlight challenges with using margin sediment δ^{66}Zn record for this purpose. Specifically, Zn isotope data in this study, together with those for other margin sediments (Little et al., 2016; Zhang et al., 2021), demonstrate that these settings exhibit patterns that do not straightforwardly reflect seawater δ^{66}Zn. In this particular context, recent studies by Sweere et al. (2018, 2020) have suggested excursions to lower seawater δ^{66}Zn values during OAE 2, linked to remobilization of isotopically light Zn from continental margin sediments, as a result of widespread seafloor re-oxygenation – a suggestion that is consistent with the release of light Zn to the water column implied by the Namibian margin porewater data (Fig. 3). Ultimately, like Mo, euxinic settings such as the Black Sea, where the removal of both Mo and Zn is close to quantitative (Neubert et al., 2008; Vance et al., 2016), are simpler situations to reconstruct ancient seawater isotope compositions of either Mo or Zn than upwelling margins (this study; Siebert et al., 2006; Poulson et al., 2006, 2009; Little et al., 2016; He et al., 2021).

6. Conclusions

In this paper we have presented new Zn and Ni concentration and isotope data for both bulk solid phase and porewater in sediments from three sites along a transect across the Namibian upwelling margin. The three objectives of this study were: (1) to understand and quantify an important sedimentary sink for Zn and Ni isotopes, that into sediments in productive upwelling margin settings; (2) to expand our understanding of the marine budgets of Zn and Ni isotopes; and (3) with a view to applications as paleoenvironment tracers. The mechanisms that control the burial and isotope compositions of Zn and Ni in sediments on the Namibian margin are illustrated schematically in Fig. 9. We find that authigenic Zn and Ni in the sediments are mainly delivered via export production from the photic zone. Authigenic Ni isotopes are very close to the deep ocean δ^{60}Ni, while authigenic δ^{66}Zn reflects diagenetic re-processing.

Porewater data are complex, probably do not always reflect steady-state profiles in equilibrium with the current redox state of the sediment-porewater system, and constitute a small pool of Zn and Ni that is very sensitive to multiple processes. Porewater Zn isotopes are most likely buffered by the dissolution of a previously-formed sulfide phase. The data suggest substantial benthic fluxes of isotopically light Zn at the time of sampling, but this must be transient as it is not consistent with the long-term burial of Zn that is lighter than the deep ocean. Porewater Ni isotopes reflect both a source of light isotopes from the dissolution of Mn oxides and the removal of light isotopes into a solid sulfide. The latter leads to residual heavy porewater Ni isotopes that points to the potential for a small benthic flux of heavy Ni isotopes back to the water column.

Our study confirms the burial of isotopically light Zn in open-margin settings, the crucial light sink for the global isotopic mass balance and the heavy isotope composition of the modern ocean. The isotope composition of sedimentary authigenic Ni, on the other hand, is the same as that of the modern deep ocean. As such, though they exert very little isotopic leverage on the global oceanic Ni budget, sediments from such settings have potential as records of the past ocean.

Declaration of Competing Interest

The authors declare that they have no known competing financial interests or personal relationships that could have appeared to influence the work reported in this paper.

Acknowledgments

We would like to thank the captain, the crew and the co-chief scientist Kurt Hanselmann, for their great work and support during the cruises on Namibia's R/V MIRABILIS. This work is financially supported by the National Natural Science Foundation of China (41991324, 42006060), China Postdoctoral Science Foundation (2020M671201), and China Scholarship Council. This work is also supported by funding from ETH Zürich and the Swiss National Science Foundation (200020-165904 and 200021-184873) to DV. We thank Leslie Robbins and two anonymous reviewers for constructive comments that improved this manuscript, and associate editor Claudine Stirling for editorial handling.

Appendix A. Supplementary material

The supplementary materials include detailed description of the Monte Carlo approach along with the supplementary figure (Figure S1) in a PDF file, and supplementary research data (i.e., the chemical and isotope compositions of bulk sediments and porewaters, authigenic Zn and Ni estimates in sediments; Tables S1–S3) in an Excel file. Supplementary material to this article can be found online at https://doi.org/10.1016/j.gca.2022.12.026.

References

Abshire, M.L., Owens, J.D., Cofrancesco, J., Inthorn, M., Riedinger, N., 2020a. Geochemical signatures of redepositional environments: The Namibian continental margin. Mari. Geol. 429, 106316.
Abshire, M.L., Romaniello, S.J., Kuzminov, A.M., Cofrancesco, J., Severmann, S., Riedinger, N., 2020b. Uranium isotopes as a proxy for primary depositional redox conditions in organic-rich marine systems. Earth Planet. Sci. Lett. 529, 115878.
Archer, C., Vance, D., Milne, A., Lohan, M.C., 2020. The oceanic biogeochemistry of nickel and its isotopes: New data from the South Atlantic and the Southern Ocean biogeochemical divide. Earth Planet. Sci. Lett. 535, 116118.
Bermin, J., Vance, D., Archer, C., Statham, P., 2006. The determination of the isotopic composition of Cu and Zn in seawater. Chem. Geol. 226, 280–297.
Böning, P., Fröllje, H., Beck, M., Schnetger, B., Brumsack, H.J., 2012. Underestimation of the authigenic fraction of Cu and Ni in organic-rich sediments. Mari. Geol. 323, 24–28.
Böning, P., Shaw, T., Pahnke, K., Brumsack, H.J., 2015. Nickel as indicator of fresh organic matter in upwelling sediments. Geochim. Cosmochim. Acta 162, 99–108.
Böning, P., Schnetger, B., Belz, L., Ferdelman, T., Brumsack, H.J., Pahnke, K., 2020. Sedimentary iron cycling in the Benguela upwelling system off Namibia. Earth Planet. Sci. Lett. 538, 116212.
Borchers, S., Schnetger, B., Böning, P., Brumsack, H.J., 2005. Geochemical signatures of the Namibian diatom belt: Perennial upwelling and intermittent anoxia. Geochem. Geophys. Geosyst. 6, Q06006.
Bremner, J., Willis, J., 1993. Mineralogy and geochemistry of the clay fraction of sediments from the Namibian continental margin and the adjacent hinterland. Mari. Geol. 115, 85–116.
Brüchert, V., Currie, B., Peard, K.R., Lass, U., Endler, R., Dübecke, A., Julies, E., Leipe, T., Zitzmann, S., 2006. Biogeochemical and physical control on shelf anoxia and water column hydrogen sulphide in the Benguela coastal upwelling system off Namibia. In: Neretin, L.N. (Ed.), Past and Present Water Column Anoxia. Springer, pp. 161–193.
Brüchert, V., Jørgensen, B.B., Neumann, K., Riechmann, D., Schlösser, M., Schulz, H., 2003. Regulation of bacterial sulfate reduction and hydrogen sulfide fluxes in the central Namibian coastal upwelling zone. Geochim. Cosmochim. Acta 67, 4505–4518.
Bruland, K.W., 1980. Oceanographic distributions of cadmium, zinc, nickel, and copper in the North Pacific. Earth Planet. Sci. Lett. 47, 176–198.
Cameron, V., Vance, D., 2014. Heavy nickel isotope compositions in rivers and the oceans. Geochim. Cosmochim. Acta 128, 195–211.
Cameron, V., Vance, D., Archer, C., House, C.H., 2009. A biomarker based on the stable isotopes of nickel. Proc. Natl. Acad. Sci. 106, 10944–10948.
Chen, X., Sageman, B.B., Yao, H., Liu, S., Han, K., Zou, Y., Wang, C., 2021. Zinc isotope evidence for paleoenvironmental changes during Cretaceous Oceanic Anoxic Event 2. Geology 49, 412–416.
Ciscato, E.R., Bontognali, T.R.R., Vance, D., 2018. Nickel and its isotopes in organic-rich sediments: implications for oceanic budgets and a potential record of ancient seawater. Earth Planet. Sci. Lett. 494, 239–250.
Conway, T.M., John, S.G., 2014. The biogeochemical cycling of zinc and zinc isotopes in the North Atlantic Ocean. Glob. Biogeochem. Cycles 28, 1111–1128.
Conway, T.M., John, S.G., 2015. The cycling of iron, zinc and cadmium in the North East Pacific Ocean – Insights from stable isotopes. Geochim. Cosmochim. Acta 164, 262–283.
Daskalakis, K.D., George, R.H., 1993. The solubility of sphalerite (ZnS) in sulfidic solutions at 25°C and 1 atm pressure. Geochim. Cosmochim. Acta 57, 4923–4931.
de Souza, G.F., Vance, D., Sieber, M., Conway, T.M., Little, S.H., 2022. Re-assessing the influence of particle-hosted sulphide precipitation on the marine cadmium cycle. Geochim. Cosmochim. Acta 322, 274–296.
Ducher, M., Blanchard, M., Balan, E., 2018. Equilibrium isotopic fractionation between aqueous Zn and minerals from first-principles calculations. Chem. Geol. 483, 342–350.
Fujii, T., Moynier, F., Dauphas, N., Abe, M., 2011. Theoretical and experimental investigation of nickel isotopic fractionation in species relevant to modern and ancient oceans. Geochim. Cosmochim. Acta 75, 469–482.
Gall, L., Williams, H., Siebert, C., Halliday, A., Herrington, R., Hein, J., 2013. Nickel isotopic compositions of ferromanganese crusts and the constancy of deep ocean inputs and continental weathering effects over the Cenozoic. Earth Planet. Sci. Lett. 375, 148–155.
Gueguen, B., Rouxel, O., Ponzevera, E., Bekker, A., Fouquet, Y., 2013. Nickel isotope variations in terrestrial silicate rocks and geological reference materials measured by MC-ICP-MS. Geostand. Geoanal. Res. 37, 297–317.
Gueguen, B., Rouxel, O., 2021. The Nickel isotope composition of the authigenic sink and the diagenetic flux in modern oceans. Chem. Geol. 563, 120050.
Gueguen, B., Rouxel, O., Rouget, M.-L., Bollinger, C., Ponzevera, E., Germain, Y., Fouquet, Y., 2016. Comparative geochemistry of four ferromanganese crusts from the Pacific Ocean and significance for the use of Ni isotopes as paleoceanographic tracers. Geochim. Cosmochim. Acta 189, 214–235.
Gueguen, B., Sorensen, J.V., Lalonde, S.V., Peña, J., Toner, B.M., Rouxel, O., 2018. Variable Ni isotope fractionation between Fe-oxyhydroxides and implications for the use of Ni isotopes as geochemical tracers. Chem. Geol. 481, 38–52.
Gueguen, B., Rouxel, O., Fouquet, Y., 2021. Nickel isotopes and rare earth elements systematics in marine hydrogenetic and hydrothermal ferromanganese deposits. Chem. Geol. 560, 119999.
Hansen, A., Ohde, T., Wasmund, N., 2014. Succession of micro- and nanoplankton groups in ageing upwelled waters off Namibia. J. Mar. Syst. 140, 130–137.
He, Z., Clarkson, M.O., Andersen, M.B., Archer, C., Sweere, T.C., Kraal, P., Guthauser, A., Huang, F., Vance, D., 2021. Temporally and spatially dynamic redox conditions on an upwelling margin: The impact on coupled sedimentary Mo and U isotope systematics, and implications for the Mo-U paleoredox proxy. Geochim. Cosmochim. Acta 309, 251–271.
Ingall, E., Jahnke, R., 1994. Evidence for enhanced phosphorus regeneration from marine sediments overlain by oxygen depleted waters. Geochim. Cosmochim. Acta 58, 2571–2575.
Inthorn, M., Mohrholz, V., Zabel, M., 2006a. Nepheloid layer distribution in the Benguela upwelling area offshore Namibia. Deep-Sea Res. I 53, 1423–1438.
Inthorn, M., Wagner, T., Scheeder, G., Zabel, M., 2006b. Lateral transport controls distribution, quality, and burial of organic matter along continental slopes in high-productivity areas. Geology 34, 205–208.
Isson, T.T., Love, G.D., Dupont, C.L., Reinhard, C.T., Zumberge, A.J., Asael, D., Gueguen, B., McCrow, J., Gill, B.C., Owens, J., Rainbird, R.H., Rooney, A.D., Zhao, M.-Y., Stueeken, E.E., Konhauser, K.O., John, S.G., Lyons, T.W., Planavsky, N.J., 2018. Tracking the rise of eukaryotes to ecological dominance with zinc isotopes. Geobiology 16, 341–352.
Janssen, D.J., Conway, T.M., John, S.G., Christian, J.R., Kramer, D.I., Pedersen, T.F., Cullen, J.T., 2014. Undocumented water column sink for cadmium in open ocean oxygen-deficient zones. Proc. Natl. Acad. Sci. 111, 6888–6893.
Janssen, D.J., Cullen, J.T., 2015. Decoupling of zinc and silicic acid in the subarctic northeast Pacific interior. Mari. Chem. 177, 124–133.
John, S.G., Conway, T.M., 2014. A role for scavenging in the marine biogeochemical cycling of zinc and zinc isotopes. Earth Planet. Sci. Lett. 394, 159–167.
John, S.G., Geis, R.W., Saito, M.A., Boyle, E.A., 2007. Zinc isotope fractionation during high-affinity and low-affinity zinc transport by the marine diatom Thalassiosira oceanica. Limnol. Oceanogr. 52, 2710–2714.
John, S.G., Kunzmann, M., Townsend, E.J., Rosenberg, A.D., 2017. Zinc and cadmium stable isotopes in the geological record: A case study from the post-snowball Earth Nuccaleena cap dolostone. Palaeogeogr. Palaeoclimatol. Palaeoecol. 466, 202–208.
John, S.G., Helgoe, J., Townsend, E., 2018. Biogeochemical cycling of Zn and Cd and their stable isotopes in the Eastern Tropical South Pacific. Mar. Chem. 201, 256–262.
John, S.G., Kelly, R.L., Bian, X., Fu, F., Smith, M.I., Lanning, N.T., Liang, H., Pasquier, B., Seelen, E.A., Holzer, M., Wasylenki, L., Conway, T.M., Fitzsimmons, J.N., Hutchins, D.A., Yang, S.-C., 2022. The biogeochemical balance of oceanic nickel cycling. Nat. Geosci. 15, 906–912.
Köbberich, M., Vance, D., 2017. Kinetic control on Zn isotope signatures recorded in marine diatoms. Geochim. Cosmochim. Acta. 210, 97–113.
Köbberich, M., Vance, D., 2019. Zn isotope fractionation during uptake into marine phytoplankton: Implications for oceanic zinc isotopes. Chem. Geol. 523, 154–161.
Konhauser, K.O., Pecoits, E., Lalonde, S.V., Papineau, D., Nisbet, E.G., Barley, M.E., Arndt, N.T., Zahnle, K., Kamber, B.S., 2009. Oceanic nickel depletion and a methanogen famine before the Great Oxidation Event. Nature 458, 750–753.
Kunzmann, M., Halverson, G.P., Sossi, P.A., Raub, T.D., Payne, J.L., Kirby, J., 2013. Zn isotope evidence for immediate resumption of primary productivity after snowball Earth. Geology 41, 27–30.

Lemaitre, N., de Souza, G.F., Archer, C., Wang, R.-M., Planquette, H., Sarthou, G., Vance, D., 2020. Pervasive sources of isotopically light zinc in the North Atlantic Ocean. Earth Planet. Sci. Lett. 539, 116216.
Lemaitre, N., Du, J.-H., de Souza, G.F., Archer, C., Vance, D., 2022. The essential bioactive role of nickel in the oceans: Evidence from nickel isotopes. Earth Planet. Sci. Lett. 584, 117513.
Li, M., Grasby, S.E., Wang, S.-J., Zhang, X., Wasylenki, L.E., Xu, Y., Sun, M., Beauchamp, B., Hu, D., Shen, Y., 2021. Nickel isotopes link Siberian Traps aerosol particles to the end-Permian mass extinction. Nat. Commun. 12, 2024.
Liao, W.-H., Takano, S., Yang, S.-C., Huang, K.-F., Sohrin, Y., Ho, T.-Y., 2020. Zn isotope composition in the water column of the northwestern Pacific ocean: the importance of external sources. Glob. Biogeochem. Cycles 34. e2019GB006379.
Little, S., Vance, D., Walker-Brown, C., Landing, W., 2014. The oceanic mass balance of copper and zinc isotopes, investigated by analysis of their inputs, and outputs to ferromanganese oxide sediments. Geochim. Cosmochim. Acta 125, 673–693.
Little, S.H., Vance, D., Lyons, T.W., McManus, J., 2015. Controls on trace metal authigenic enrichment in reducing sediments: Insights from modern oxygen-deficient settings. Am. J. Sci. 315, 77–119.
Little, S.H., Vance, D., McManus, J., Severmann, S., 2016. Key role of continental margin sediments in the oceanic mass balance of Zn and Zn isotopes. Geology 44, 207–210.
Little, S.H., Archer, C., McManus, J., Najorka, J., Wegorzewski, A.V., Vance, D., 2020. Towards balancing the oceanic Ni budget. Earth Planet. Sci. Lett. 547, 116461.
Liu, S.-A., Wu, H., Shen, S.-Z., Jiang, G., Zhang, S., Lv, Y., Zhang, H., Li, S., 2017. Zinc isotope evidence for intensive magmatism immediately before the end-Permian mass extinction. Geology 45, 343–346.
Manheim, F.T., Lane-Bostwick, C.M., 1989. Chemical composition of ferromanganese crusts in the world ocean: a review and comprehensive database, Open-File Report, First posted 1989; Revised and reposted November 18, 2014, version 1.1 ed, U.S. Geological Survey, Woods Hole, MA, p. 480.
Maréchal, C.N., Nicolas, E., Douchet, C., Albarède, F., 2000. Abundance of zinc isotopes as a marine biogeochemical tracer. Geochem. Geophys. Geosyst. 1. 1999GC–000029.
Middag, R., de Baar, H.J.W., Bruland, K.W., van Heuven, S.M.A.C., 2020. The distribution of nickel in the West-Atlantic Ocean, its relationship with phosphate and a comparison to cadmium and zinc. Front. Mar. Sci. 7, 105.
Mohrholz, V., Bartholomae, C.H., van der Plas, A.K., Lass, H.U., 2008. The seasonal variability of the northern Benguela undercurrent and its relation to the oxygen budget on the shelf. Cont. Shelf Res. 28, 424–441.
Mollenhauer, G., Schneider, R.R., Müller, P.J., Spieß, V., Wefer, G., 2002. Glacial/interglacial variablity in the Benguela upwelling system: Spatial distribution and budgets of organic carbon accumulation. Glob. Biogeochem. Cycles 16, 1134.
Monteiro, P.M.S., van der Plas, A., Mohrholz, V., Mabille, E., Pascall, A., Joubert, W., 2006. Variability of natural hypoxia and methane in a coastal upwelling system: Oceanic physics or shelf biology? Geophys. Res. Lett. 33, L16614.
Morel, F.M.M., Milligan, A.J., Saito, M.A., 2014. Marine bioinorganic chemistry: the role of trace metals in the oceanic cycles of the major nutrients. Treatise Geochem. 8, 123–150.
Morel, F.M., Price, N., 2003. The biogeochemical cycles of trace metals in the oceans. Science 300, 944–947.
Morse, J.W., Luther, G.W., 1999. Chemical influences on trace metal-sulfide interactions in anoxic sediments. Geochim. Cosmochim. Acta 63, 3373–3378.
Moynier, F., Vance, D., Fujii, T., Savage, P., 2017. The Isotope Geochemistry of Zinc and Copper. Rev. Mineral. Geochem. 82, 543–600.
Müsing, K., Clarkson, M.O., Vance, D., 2022. The meaning of carbonate Zn isotope records: Constraints from a detailed geochemical and isotope study of bulk deep-sea carbonates. Geochim. Cosmochim. Acta 324, 26–43.
Nagel, B., Emeis, K.C., Flohr, A., Rixen, T., Schlarbaum, T., Mohrholz, V., Plas, A., 2013. N-cycling and balancing of the N-deficit generated in the oxygen minimum zone over the Namibian shelf—An isotope-based approach. J. Geophys. Res. Biogeosci. 118, 361–371.
Nelson, G., Hutchings, L., 1983. The Benguela upwelling area. Prog. Oceanogr. 12, 333–356.
Neubert, N., Nägler, T.F., Böttcher, M.E., 2008. Sulfidity controls molybdenum isotope fractionation into euxinic sediments: Evidence from the modern Black Sea. Geology 36, 775–778.
Paytan, A., McLaughlin, K., 2007. The oceanic phosphorus cycle. Chem. Rev. 107, 563–576.
Plass, A., Dale, A.W., Scholz, F., 2021. Sedimentary cycling and benthic fluxes of manganese, cobalt, nickel, copper, zinc and cadmium in the Peruvian oxygen minimum zone. Mari. Chem. 233, 103982.
Poulson Brucker, R.L., McManus, J., Severmann, S., Berelson, W.M., 2009. Molybdenum behavior during early diagenesis: Insights from Mo isotopes. Geochem. Geophys. Geosyst. 10.
Poulson, R.L., Siebert, C., McManus, J., Berelson, W.M., 2006. Authigenic molybdenum isotope signatures in marine sediments. Geology 34, 617–620.
Ragsdale, S.W., 2009. Nickel-based Enzyme Systems. J. Biol. Chem. 284, 18571–18575.
Revels, B.N., Rickli, J., Moura, C.A.V., Vance, D., 2021. Nickel and its isotopes in the Amazon Basin: the impact of the weathering regime and delivery to the oceans. Geochim. Cosmochim. Acta. 293, 344–364.
Rudnick, R.L., Gao, S., 2003. Composition of the continental crust. In: Holland, H.D., Turekian, K.K. (Eds.), Treatise on Geochemistry. Elsevier-Pergamon, Oxford, pp. 1–64.
Samanta, M., Ellwood, M.J., Sinoir, M., Hassler, C.S., 2017. Dissolved zinc isotope cycling in the Tasman Sea, SW Pacific Ocean. Mari. Chem. 192, 1–12.
Shannon, L.V., Nelson, G., 1996. The Benguela: Large Scale Features and Processes and System Variability. In: Wefer, G., Berger, W.H., Siedler, G., Webb, D.J. (Eds.), The South Atlantic: Present and Past Circulation. Springer, Berlin Heidelberg, pp. 163–210.
Sieber, M., Conway, T.M., de Souza, G.F., Hassler, C.S., Ellwood, M.J., Vance, D., 2020. Cycling of zinc and its isotopes across multiple zones of the Southern Ocean: Insights from the Antarctic Circumnavigation Expedition. Geochim. Cosmochim. Acta 268, 310–324.
Siebert, C., McManus, J., Bice, A., Poulson, R., Berelson, W.M., 2006. Molybdenum isotope signatures in continental margin marine sediments. Earth Planet. Sci. Lett. 241, 723–733.
Sorensen, J.V., Gueguen, B., Stewart, B.D., Peña, J., Rouxel, O., Toner, B.M., 2020. Large nickel isotope fractionation caused by surface complexation reactions with hexagonal birnessite. Chem. Geol. 537, 119481.
Sun, M., Archer, C., Vance, D., 2021. New methods for the chemical isolation and stable isotope measurement of multiple transition metals, with application to the earth sciences. Geostand. Geoanal. Res. 45, 643–658.
Sweere, T.C., Dickson, A.J., Jenkyns, H.C., Porcelli, D., Elrick, M., van den Boorn, S.H., Henderson, G.M., 2018. Isotopic evidence for changes in the zinc cycle during Oceanic Anoxic Event 2 (Late Cretaceous). Geology 46, 463–466.
Sweere, T.C., Dickson, A.J., Jenkyns, H.C., Porcelli, D., Henderson, G.M., 2020. Zinc- and cadmium-isotope evidence for redox-driven perturbations to global micronutrient cycles during Oceanic Anoxic Event 2 (Late Cretaceous). Earth Planet. Sci. Lett. 546, 116427.
Takano, S., Tanimizu, M., Hirata, T., Sohrin, Y., 2013. Determination of isotopic composition of dissolved copper in seawater by multi-collector inductively coupled plasma mass spectrometry after pre-concentration using an ethylenediaminetriacetic acid chelating resin. Anal. Chim. Acta 784, 33–41.
Takano, S., Tanimizu, M., Hirata, T., Shin, K.-C., Fukami, Y., Suzuki, K., Sohrin, Y., 2017. A simple and rapid method for isotopic analysis of nickel, copper, and zinc in seawater using chelating extraction and anion exchange. Anal. Chim. Acta 967, 1–11.
Tribovillard, N., Algeo, T.J., Lyons, T., Riboulleau, A., 2006. Trace metals as paleoredox and paleoproductivity proxies: an update. Chem. Geol. 232, 12–32.
Twining, B.S., Baines, S.B., 2013. The Trace Metal Composition of Marine Phytoplankton. In: Carlson, C.A., Giovannoni, S.J. (Eds.), *Annu. Rev. Mar. Sci.* **5**, 191–215.
Twining, B.S., Nunez-Milland, D., Vogt, S., Johnson, R.S., Sedwick, P.N., 2010. Variations in Synechococcus cell quotas of phosphorus, sulfur, manganese, iron, nickel, and zinc within mesoscale eddies in the Sargasso Sea. Limnol. Oceanogr. 55, 492–506.
Twining, B.S., Baines, S.B., Vogt, S., Nelson, D.M., 2012. Role of diatoms in nickel biogeochemistry in the ocean. Glob. Biogeochem. Cycles 26, GB4001.
Vance, D., Little, S.H., Archer, C., Cameron, V., Andersen, M.B., Rijkenberg, M.J., Lyons, T.W., 2016. The oceanic budgets of nickel and zinc isotopes: the importance of sulfidic environments as illustrated by the Black Sea. Phil. Trans. R. Soc. A 374, 20150294.
Vance, D., de Souza, G.F., Zhao, Y., Cullen, J.T., Lohan, M.C., 2019. The relationship between zinc, its isotopes, and the major nutrients in the North-East Pacific. Earth Planet. Sci. Lett. 525, 115748.
Wang, R.M., Archer, C., Bowie, A.R., Vance, D., 2019b. Zinc and nickel isotopes in seawater from the Indian Sector of the Southern Ocean: The impact of natural iron fertilization versus Southern Ocean hydrography and biogeochemistry. Chem. Geol. 511, 452–464.
Wang, S.-J., Rudnick, R.L., Gaschnig, R.M., Wang, H., Wasylenki, L.E., 2019a. Methanogenesis sustained by sulfide weathering during the Great Oxidation Event. Nat. Geosci. 12, 296–300.
Weber, T., John, S., Tagliabue, A., DeVries, T., 2018. Biological uptake and reversible scavenging of zinc in the global ocean. Science 361, 72–76.
Weeks, S.J., Currie, B., Bakun, A., Peard, K.R., 2004. Hydrogen sulphide eruptions in the Atlantic Ocean off southern Africa: implications of a new view based on SeaWiFS satellite imagery. Deep-Sea Res. Part I 51, 153–172.
Yan, B., Zhu, X., He, X., Tang, S., 2019. Zn isotopic evolution in early Ediacaran ocean: A global signature. Precambrian Res. 320, 472–483.
Yang, S.-C., Hawco, N.J., Gonzalez, P.P., Bian, X., Huang, K.-F., Zhang, R., John, S.G., 2020. A new purification method for Ni and Cu stable isotopes in seawater provides evidence for widespread Ni isotope fractionation by phytoplankton in the North Pacific. Chem. Geol. 547, 119662.
Yang, S.-C., Kelly, R.L., Bian, X., Conway, T.M., Huang, K.-F., Ho, T.-Y., Neibauer, J.A., Keil, R.G., Moffett, J.W., John, S.G., 2021. Lack of redox cycling for nickel in the water column of the Eastern tropical north pacific oxygen deficient zone: Insight from dissolved and particulate nickel isotopes. Geochim. Cosmochim. Acta. 309, 235–250.
Zhang, Y., Planavsky, N.J., Zhao, M., Isson, T., Asael, D., Wang, C., Wang, F., 2021. The isotopic composition of sedimentary organic zinc and implications for the global Zn isotope mass balance. Geochim. Cosmochim. Acta. 314, 16–26.
Zhao, Z., Shen, B., Zhu, J.-M., Lang, X., Wu, G., Tan, D., Pei, H., Huang, T., Ning, M., Ma, H., 2021. Active methanogenesis during the melting of Marinoan snowball Earth. Nat. Commun. 12, 955.
Zhao, Y., Vance, D., Abouchami, W., De Baar, H., 2014. Biogeochemical cycling of zinc and its isotopes in the Southern Ocean. Geochim. Cosmochim. Acta 125, 653–672.